AALBORG UNIVERSITY
STUDENT REPORT

Fatigue analysis of offshore transport equipment

Project Report
BM4-5

Department of Civil Engineering
Aalborg University Esbjerg
Denmark

AALBORG UNIVERSITY
STUDENT REPORT

Byggeri og Anlæg
Aalborg University
http://www.aau.dk

Title:
Fatigue analysis of offshore transport equipment

Theme:
Fatigue analysis of offshore structures

Project Period:
01/09/20 - 10/06/21

Project Group:
BM4-5

Participant:
Nikolaj Bruun

Supervisors:
Professor Lars Damkilde
Jonas Madsen (MAST Engineering)

Page Numbers: 114

Date of Completion:
June 10, 2021

Abstract:

This project investigates the different methods used for determining the stress range used in fatigue calculations. The focus is to investigate the fatigue damage in welded connection. First, a global beam model was used to identify the governing load case before using ANSYS Workbench. Then, the fatigue damage was compared based on the stress range determine in the ANSYS Workbench model. This analysis aims to determine how the stress assessment has influenced the fatigue damage and the process used to determine the stress range by finite element. The stress ranges were then used to determine the fatigue damage based on the simplified fatigue assessment method by two-parameter Weibull distribution. The results provided hereby are also compared, finally argued, and the deviation between the outcome of the different approaches is debate.

Contents

Preface

Mechanical Design at Aalborg University Esbjerg.
The theme of the report is offshore sea transport structures, where the aim is to investigate fatigue damage based on different fatigue assessment methods by finite elements.

The structure of the report is given as:

- Chapters are indicated as X
- Sections are indicated as X.X
- Subsections are indicated as X.X.X

All equations are enumerated throughout the text by chapter and are referred to as (chapter. equation). All figures are similarly numbered and indicated as (chapter. figure). Citations are specified with the use of square brackets [] and can be found with the same number in the bibliography. Vectors and matrices are denoted with bold characters.

During the writing of the report, the following software were used:

- LaTeX Overleaf
- MATLAB r2019a
- ANSYS Workbench 19.0
- Autodesk Inventor 2021
- Autodesk AutoCAD 2021
- Autodesk ROBOT 2021

All virtual files produced in Excel, Autodesk files, ANSYS Workbench, can be found in Appendix A. This project uses several standards to determine load cases, design conditions and general guidelines to verify the project statement. The standards used throughout the report are listed in Tb. 1.1, and numerated as [A-G].

Acknowledgments

I would like to thank my supervision, Professor Lars Damkilde. I am grateful to have had him as my main supervisor during my study as Master student and at this Master Thesis. Furthermore, thanks are given to M.Sc.Mech.Eng Jonas Madsen, senior structural engineer at MAST Engineering and M.Sc.Mech.Eng Maximilian Kosmale, team leader at Siemens Gamesa for the contributions from both are highly appreciated. Special gratitude is directed to M.Sc.Mech.Eng Troels Juhl Kristensen senior structural engineer at ON2A4 for guidance and help with Autodesk ROBOT. Special thanks is given to M.Sc.Mech.Eng Morten Fogh Jacobsen, senior structural engineer at R&D for valid discussions on the topic of which the thesis revolves. Finally, thanks for the cooperation between Aalborg University and Siemens Gamesa Renewable Energy.

Nikolaj Bruun

Nikolaj Bruun
<noab11@student.aau.dk>

Aalborg University Esbjerg, June 10, 2021

Chapter 1

Introduction

The objective is to investigate the methods used for determining the stress range used in fatigue damage calculation, in cooperation with Siemens Gamesa Renewable Energy (SGRE). The purpose is to evaluate the fatigue damage based on two setups in ANSYS models, one with and one without the weld geometry. The two setups are used for comparison of different stress range methods. The second part is that SGRE wants to implement beam software during the global analysis of equipment to limit the use of the 3D model in ANSYS Workbench. The equipment department is responsible for developing transport, storage and lifting equipment for components used in offshore wind turbines.

With the increasing focus on renewable energy, wind turbines have been growing significantly in size and weight in recent years. This effect has increased the capacity of wind turbines dramatically. The offshore wind turbines advantages are the high potential wind energy and larger scaled projects compared with onshore wind turbines.

The largest offshore wind turbine developed by SGRE in 2021 has a capacity of 14 MW, and a rotor diameter of 222 m [1]. The increasing dimension of the offshore wind turbine has meet the limits of todays road transportation infrastructure because it requires route improvements, cutting trees or removing trees, signs, buildings and bridges. The offshore wind turbine manufacturers is now relocated to quayside factorys.

In 2018 SGRE invested in the largest production for assembly of generators, hubs and nacelle for offshore wind turbines at Cuxhaven in Germany. SGRE is increasing the offshore production for blades at Port of Hull at Alexandra Dock in England [2]. The reason is to have a direct transportation method for offshore wind turbine components by vessel from the quayside factory to the port site, the locations are depicted in Fig. 1.1.

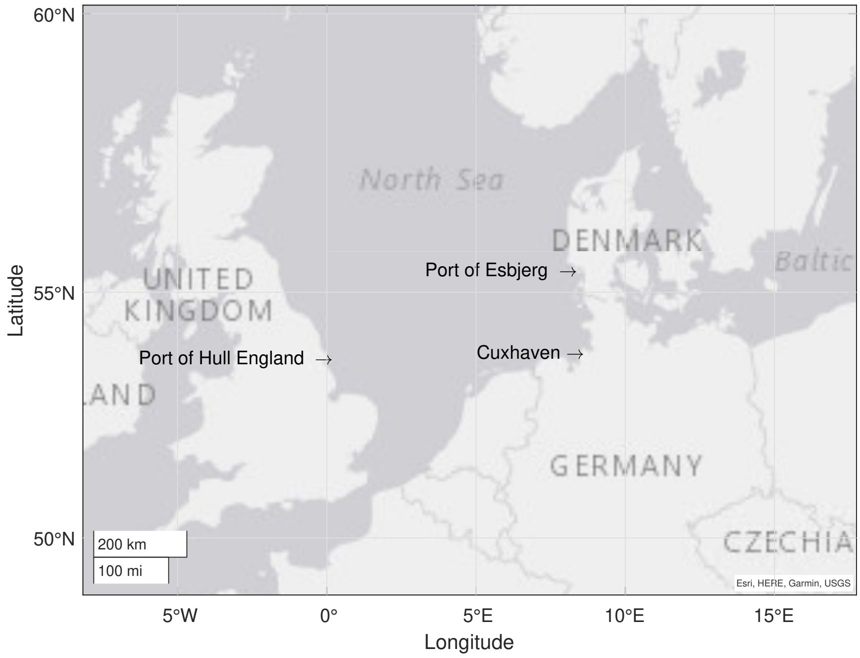

Figure 1.1: An overview over the locations, Cuxhaven, Port of Esbjerg and Port of Hull, England.

1.1 Offshore wind turbine

Offshore wind turbine, depicted in Fig. 1.2, exploits the wind energy to produce electricity. Before the wind turbine can produce electricity, it must be manufactured, transported, assembled and installed at the wind farm. The wind turbine is transported as nacelles, generators, hubs, blades and tower sections as (bottom, middle and top section).

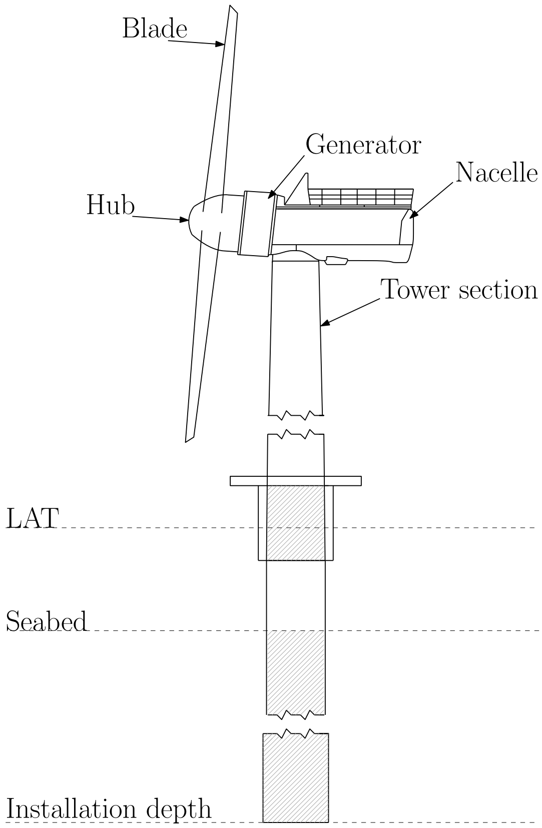

Figure 1.2: An overview of the main components in a typical wind turbines.

Transport of wind turbine components can be done separately or assembled as nacelle with a generator, illustrated in Fig. 1.3. For each wind turbine component, a separate transport frame is required. In some cases, the transport frame is also verified for short-term storage, road transport and lifting. The connections between the transport equipment and the nacelle, hub and tower is a bolted connection. In some cases, an adaptor between hub and transport frame is required because of shifting bolt pattern or various bolt flange interface diameters, illustrated in Fig. 1.3a.

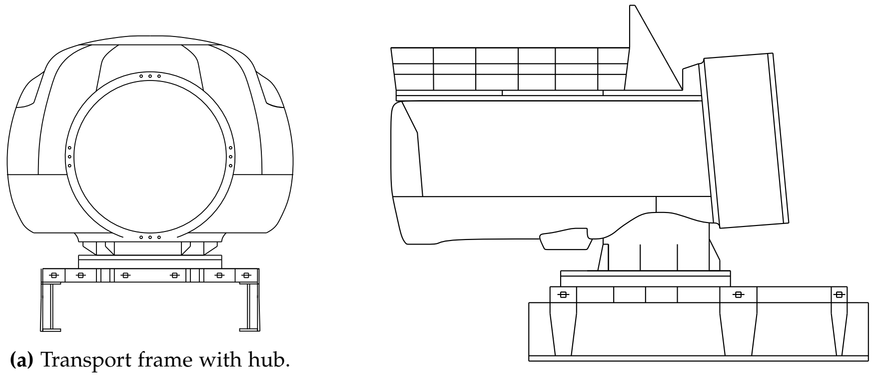

(a) Transport frame with hub.

(b) Transport frame with nacelle and generator.

Figure 1.3: Transport equipment for hub and nacelle with generator.

For blade transportation, illustrated in Fig. 1.4, it requires support at root-end and tip-end. The root-end is assembled together with the blade bolt pattern, where the root-end function is fixed support during transport.

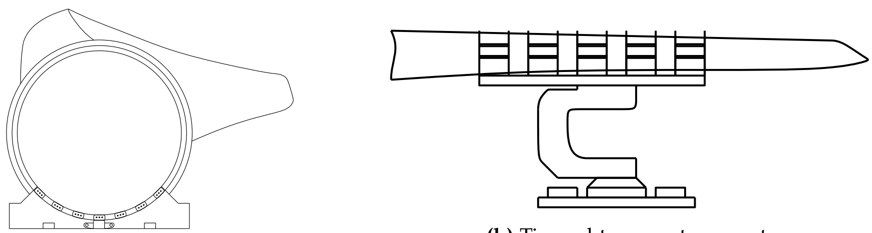

(a) Root-end transport support.

(b) Tip-end transport support.

Figure 1.4: Transport equipment for blade transportation.

The tip-end support functions are to support the blade and protect it from damage, and it has the freedom to move and rotate. The tip-end is a mechanical system with a locking system that clamps around the blade. The blade support design phase is time-consuming and complex due to two supports, the mechanic and load cases. In some cases, it requires that the support is also verified for road and lifting with the specifications that the blade system can be stacked with three blades.

For transporting of tower sections, illustrated in Fig. 1.5, this is done separately due to the length of the bottom, middle and the top tower section. When transporting tower sections, it requires support at both ends. The connections between the tower section and support is a bolt connection.

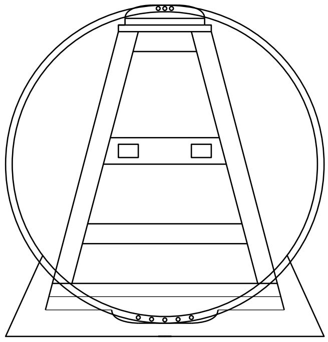

Figure 1.5: Transport frame for transport of tower sections.

When transporting blade with jack-up, it is done with a blade rack, illustrated in Fig. 1.6. The blade rack has two modules, root-end and tip-end. The blade can be stacked in a blade rack with a minimum of three blades. The blade rack is fixed to the vessel deck. When the vessel is sailing, the blade will deflect due to the elastic material. The designer must ensure that the wave is not damaging the blade, as illustrated in Fig. 1.6b.

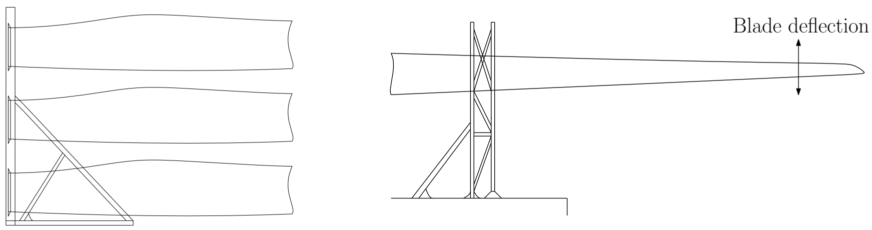

(a) Blade rack root-end support.

(b) Blade rack tip support.

Figure 1.6: An overview of the main components in a typical blade rack.

When using the installations vessel as a transport method, the failure mode is the fatigue damage due to wave loading. The analysis phase of sea equipment is complex and time-consuming. There are potential in optimising the process based on the methodology used to analyse the stress range that causes the fatigue damage. If the concept of introducing a simplified beam model in the design phase. This can lead to more optimised transport equipment due to minimising the time used in solving the ANSYS model, and the designer can have a focus on the global model in beam software where the designer can optimise the model based on the overall utilisation of members before using ANSYS Workbench to detailed analysis.

1.2 Sea transport of wind turbine components

For transporting of wind turbine components, different types of vessels are used in the marine operations. The roll-on/roll-off (RO/RO) vessel are designed to carry heavy cargoes as wind turbines components, illustrated in Fig. 1.7. The loading of nacelles are done by self-propelled modular transporter (SPMT) via the hydraulic ramp system [3]. When the vessel is sailing from one geographical location to another is defined as transit conditions.

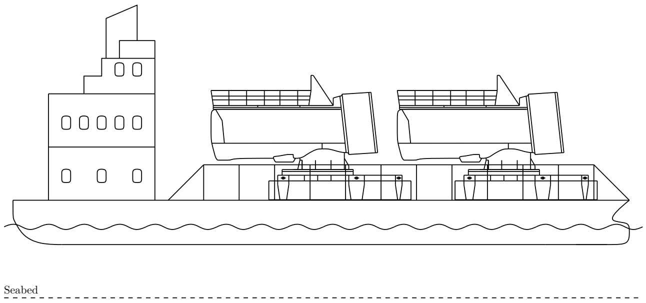

Figure 1.7: Roll-on and roll off-vessel.

The lift-on/lift-off (LO/LO) vessel is also designed to carry wind turbine components, illustrated in Fig. 1.8. The LO/LO vessel use one crane or other lift to load the equipment on board [4]. All transport equipment is designed with lifting points for handling the transport equipment with and without the wind turbine component.

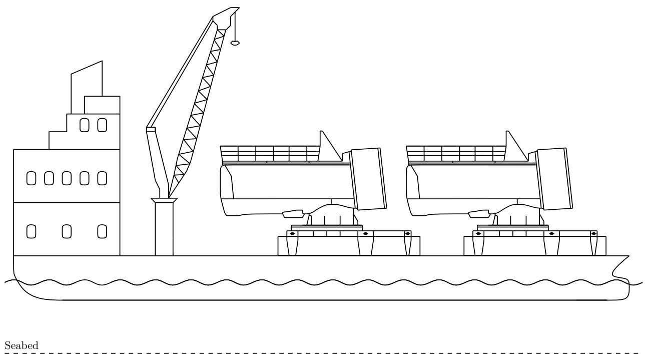

Figure 1.8: Lift-on and lift-off vessel.

The jack-up vessel (Windcarrier) illustrated in Fig. 1.9 is designed to carry wind turbines for offshore installation, where a hydraulic system controls the legs. The windcarrier can carry up to four wind turbine generator (WTG) with blades [5].

The installation at sea is complicated and highly expensive due to restricting weather time window.

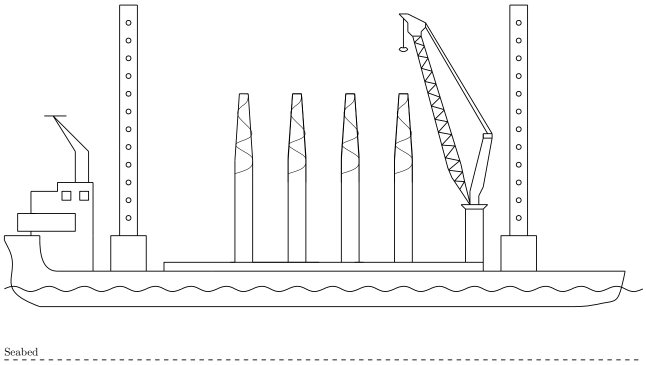

Figure 1.9: Jack-up vessel, (Windcarrier).

The elevated phase is when the windcarrier is jacking up, illustrated in Fig. 1.10, the vessel accelerations are not included only the gravity and wind load. The wind load chance due to increments in the height where this height includes the air gap of the vessel. The gravity acceleration is constant, and the only change in loads sign is the wind.

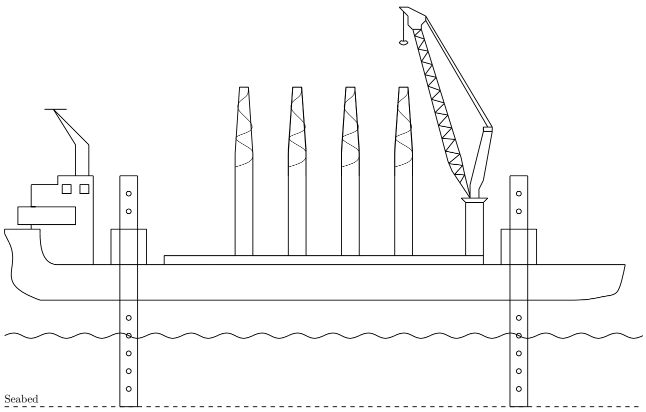

Figure 1.10: Windcarry, elevated phase.

As shown in this section, the vessel used for marine transport vary. The acceleration that the transport frame is exposed to depends on the vessel dimension and sea state. When analysing transport equipment, a transport strategy is created based on a generic selected vessel. The generic selected vessel is typical for different RO/RO or LO/LO vessels, where the highest accelerations are used in the design process. For the specific transporting with windcarrier, this types of sea transport are more influenced on the numbers of WTG and sea state.

In this master thesis, the accelerations are based on a generic transporting strategy, where the main focus is to determine the stress range and estimate the fatigue damage based on the simplified fatigue theory.

1.3 Design codes

The main code used in this thesis is DNVGL-RP-C203 (Fatigue design of offshore steel structure), which is a recommended practice for used for fatigue damage. Design code is used to ensure the integrity of the structure based on the material properties. The design code can be broken into two main categories for structure and material, and it also varies based on the continent. The environments used is for air, free corrosion in seawater and cathodic protection in seawater. The code used for design offshore transport equipment is listed in Tb. 1.1.

The main code used for the design of transport equipment for marine operation is based on DNVGL-ST-N001. The code used to ensure correct material properties is according to EN 10025-2.

Table 1.1: Standards.

Code/standard	Title	Ref
DNVGL-ST-N001	Marine operations and marine warranty	A
DNV-RP-C203	Fatigue design of offshore steel structures	B
DNV-RP-C205	Environmental conditions and environmental loads	C
DNVGL-OS-C101	Design of offshore steel structures LRFD method	D
DNVGL-CN-30.7	Fatigue Assessment of Ship Structures	E
DNVGL-RU-SHIP Pt.3 Ch.3	DNV-GL Rules for the Classification	F
IIW-2259-15	Recommendations for Fatigue	G
EN 10025-2	Eurocode 2: Hot rolled products of structural steels	H

1.4 Problem analysis

The current methodology used for analysing transport equipment is done by three-dimensional elements in ANSYS Workbench. This is intensive and time-consuming. The design process for transport equipment for nacelle transport presented in Fig. 1.11. The iterative process is presented as a flowchart in Appendix B. Where the finite element model is updated based on the utilisation of the details. However, the use of ANSYS to identify the governing load case takes significantly more time to pre-process the finite element model. It takes between two hours to seven hours or even more depending on the numbers of elements, nodes and non-linear contact as friction contact. It is also easier to unintentionally incorporate mistakes, which can be difficult to troubleshoot.

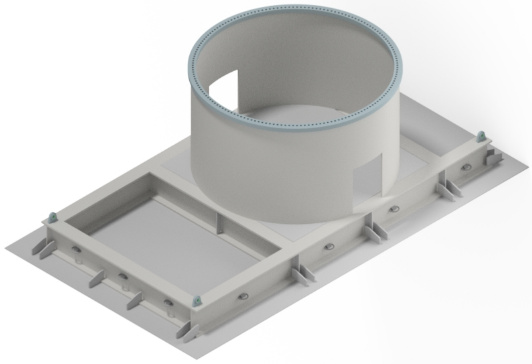

Figure 1.11: Detailed transport frame.

The fatigue damage is estimated by the simplified fatigue assessment method based on two-parameter Weibull distribution. Where the highest equivalent weld stress is used to determine the stress ranges by multiply the equivalent weld stress with two. This solution can lead to conservative weld and structure design, where the weld size is increases, because the structure detailed can not withstand the stress ranges.

In this master thesis, this problem will be solved by modelling the transport with beam elements, as presented in Fig. 1.12. The beam model is used to analyse the overall strength of the selected members of each beam elements. When the results from the beam model is sufficient, the next step is to identify the governing load cases before the details are analysed in ANSYS workbench.

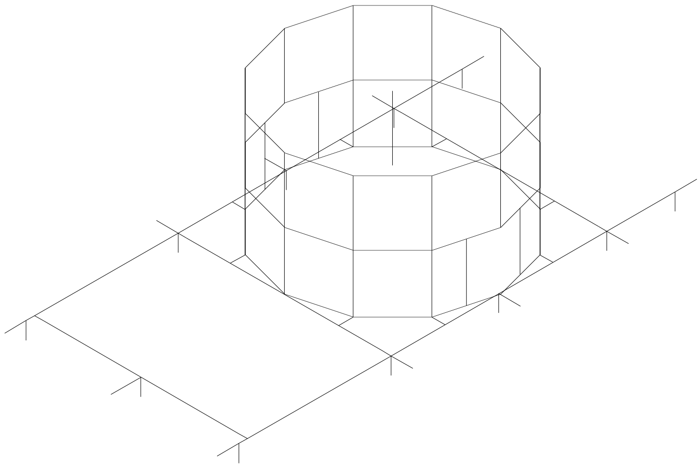

Figure 1.12: Transport frame as simple beam model.

To solve this challenge, several tools must be developed that can create the governing load cases and insert the design loads in beam software. This tool is created in Excel, which allowed the designer to easily defined load combinations that can be copied from Excel sheet to beam software. The tool used to determine the stress ranges in the weld connections is also developed, which making it smooth to identify the governing weld connection used to estimate the fatigue damage. The last task is to develop a tool for fatigue damage based on the simplified fatigue assessment by a two-parameter Weibull distribution.

The main question to be answered in this thesis is that methodology used with two times the stress to determine the stress ranges is sufficient or a more realistic method for determining the stress range for fatigue damage calculations.

Finally, an evaluation of fatigue stress assessment methods and a detailed comparison is created to show where the opportunities and constraints lie in implementing the beam software and the fatigue knowledge.

1.5 Thesis outline

Based on the problem analysis, the following plan of action has been specified in Fig. 1.13. The order of the points corresponds to the order in which this thesis is carried out. The following action is needed to understand the process of analysing transport equipment for offshore sea transport.

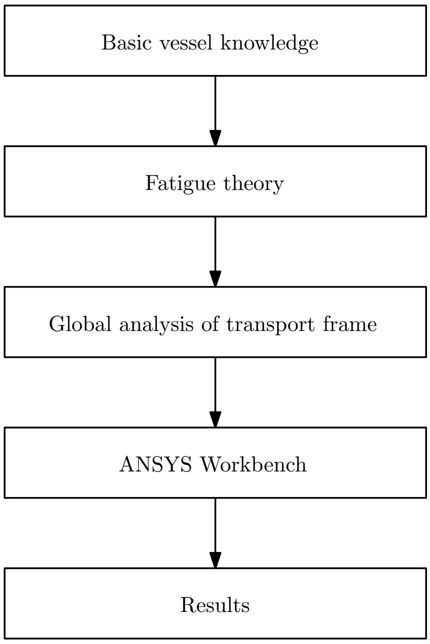

Figure 1.13: Outline of the Master thesis.

The first step is the basic knowledge regarding offshore wind turbine, sea transport and the design loads during transport. Welded connections are common locations of fatigue, where the stresses are concentrations due to geometry change.

Afterwards, the fatigue theory is described, the most used fatigue assessments methods for determining the stresses is reviewed. Finally, the transport equipment is simplified in a global model used to screen all load cases for sea transport.

After the governing load case has been selected, the detailed analysis is solved in ANSYS Workbench, and the ANSYS model is used to determine the stress range based on different methods. The last part of this master thesis is to present the results as fatigue damage, where the stress range is used with the simplified fatigue assessment method

Chapter 2

Basic vessel knowledge

This chapter introduces the basic terminology for ships/vessels. Where it covers the behaviour of the vessel during the voyage, motions, accelerations and deflection of the vessel. The deck of vessel is used to assembled the transport frame with sea fating equipment. Furthermore practical information regarding sailing route and marine operation are reviewed.

2.1 Vessel motions

A vessel with steady forward speed and irregular sea sate will oscillate in six degrees of freedom (DOF), illustrated in Fig. 2.1. The y-axis is from the stern toward the front, and the x-axis is along with breadth towards the port side [6].

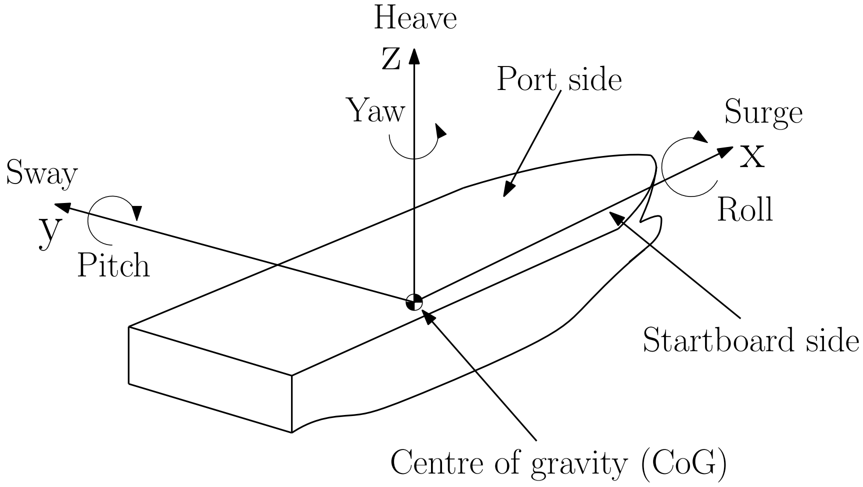

Figure 2.1: An overview of the vessel coordinate system.

Where the axis is defined as:

- The x-axis is the longitudinal axis of the vessel, positive forward.
- The y-axis is the transverse axis of the vessel, positive to portside.
- The z-axis is the vertical axis of the vessel, positive upward.

The DOFs are now split into three translation degrees, where the heaving is vertical movement when the vessel is lowering and rising. Surging is when the vessel is moving forwards or backwards based on the longitudinal axis. Swaying are the transverse movement when the vessel is moving side to side based on the transverse axis. There can also be a combined surging and swaying, and this can create a twist.

- Surge, along the x-axis, positive in positive y-direction.
- Sway, along the y-axis, positive in positive x-direction.
- Heave, along the z-axis, positive in positive z-direction.

The three last DOFs is the rotation motions known as yawing, rolling and pitching. The yaw motions are the rotation around the z-axis. The rolling is the rotation around the x-axis, and the pitching is the rotation around the y-axis.

- Roll, around the x-axis, starboard down positive.
- Pitch, around the y-axis, bow down positive.
- Yaw, around the z-axis, bow portside positive.

The headings and wave directions are related to the CoG of the vessel, illustrated in Fig. 2.2. The zero headings refer to stern waves where 90 deg is heading, or direction refers to waves from starboard. The rotation is clockwise from the centre line, and it is positive, where counter lock wise is negative rotation.

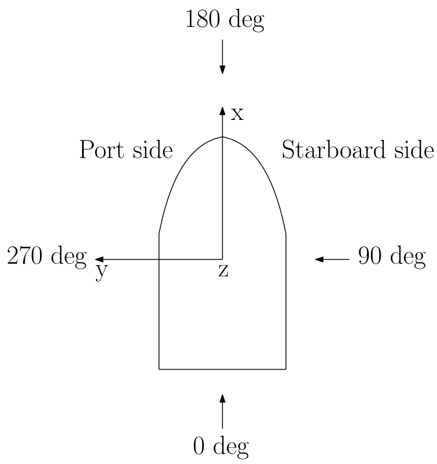

Figure 2.2: Definition of vessel heading.

2.2 Vessel deflection

For the hull girder vessel, in the basic viewpoint, illustrated in Fig. 2.3, there are mainly two loads. The weight of the vessel was acting downwards and distributed over the entire length of the vessel. The second load is the buoyancy force from the water exert on the vessels underwater body, where it acted upwards and distributed over the length of the underwater portion of the vessel.

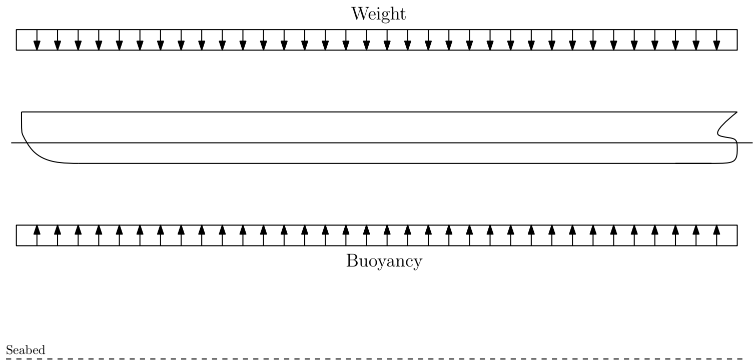

Figure 2.3: Vessel loads.

As illustrated buoyancy, (Hydrostatic external load) is the upwards force exerted by water on the vessel. When the vessel is in equilibrium, the weight is equal to its buoyancy. It must be noted that the buoyancy force distribution depends on the profile of the vessel. It keeps changing because the vessel is encountering different wave sizes. When the vessel is subjected to wave as depicted in Fig. 2.4, where the wave crest at the bow and stern. Sagging simply means that the ship is bending down at the middle

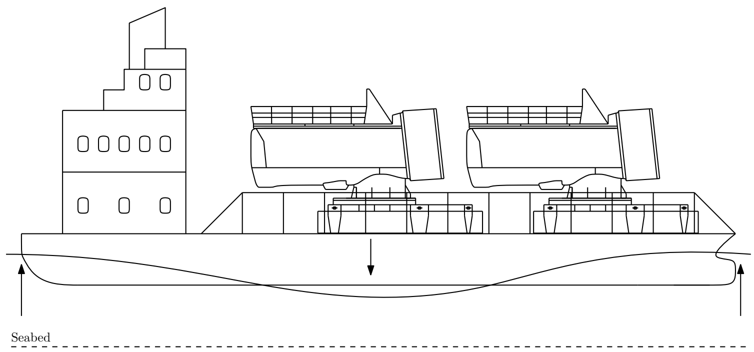

Figure 2.4: Vessel - Sagging.

If the vessel is subjected to wave as depicted in Fig. 2.5, where the wave crest is middle of the vessel, hence hogging. The wave is pushing up in the middle and give the vessel a negative curvature.

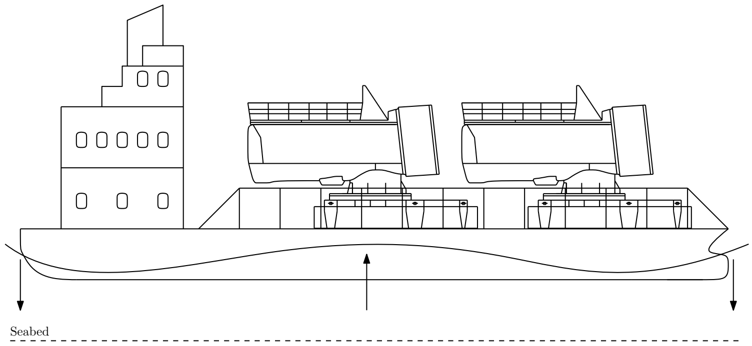

Figure 2.5: Vessel - Hogging.

When the vessel is subjected to righting moments of opposite direction at its ends, depicted in Fig. 2.6, it will twist the hull and create a torsion moment.

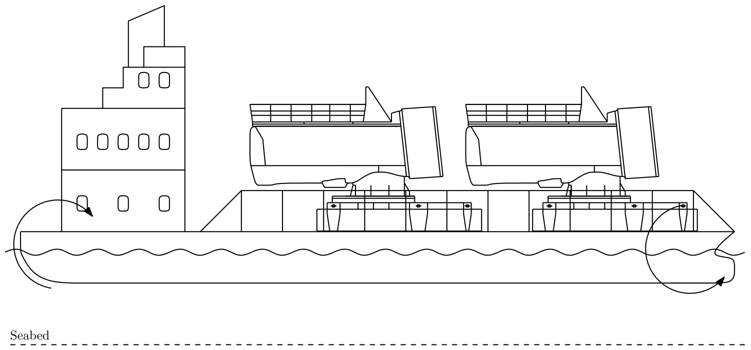

Figure 2.6: Vessel - Twist.

The effect of sagging, hogging, and torsion is not included in typical RO/RO or LO/LO vessel transport. It good practice to design sea-fastening structures to avoid transferring hull load to the transported component. It is included in more complex marine operations as installations of wind turbines. The effect from the assembled tower section on vessel grillage or blade rack can increase the overall stress on the hull section due to sagging and hogging. In some cases, the equipment allows for movement to avoid hull deflection loads are transferred into the transported component.

2.3 Vessel accelerations

There are different methods for estimating the motions and accelerations on the vessel, listed below:

- Motion analysis (Hydrodynamic software (ANSYS Aqwa or DNV HydroD)).
- Default motion criteria: [A - DNVGL-ST-N001 (Marine operations and marine warranty)].
- Default motion criteria: [F - DNV-GL Rules for the Classification of Ships, /36/, Part 3, Chapter 4].
- Alternative Methods:
  - Default motion criteria: Allowable Stress Design (ASD) / Working Stress Design (WSD) - [A - DNVGL-ST-N001, Sec. 11.7.2]
  - Default motion criteria: Load resistance factor design (LRFD) - [A - DNVGL-ST-N001, Sec. 11.7.3]

The first method is to perform a motion analysis for the vessel. The detailed motions analysis require preparing a hydrodynamic model of the vessel and applying the environmental forces. The hydrodynamic model is based on the wet surface of the hull where the hull is modelled based on the hull drawings, illustrated in Fig. 2.7a.

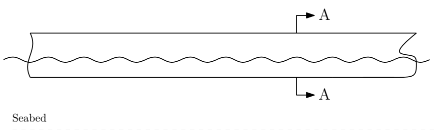

(a) Vessel surface.

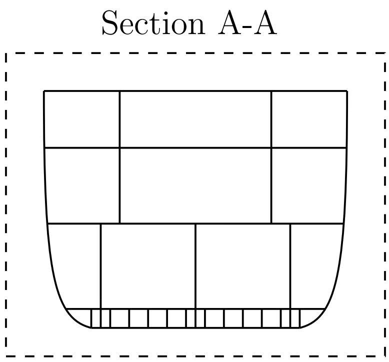

(b) Hull section for vessel.

Figure 2.7: Motion analysis for hull vessel.

The motion response analysis is used to determine design motion and accelerations action on different components as sea-fastening and transport equipment. The response analysis can be performed in the frequency domain or time domain for irregular sea states based on wave spectrum. Combined with short term statistics, this can be used to determine the maximum responses for the vessel. This is used to generate the vessel response amplitude operators (ROA).

The parameters used in response analysis is loading condition, numbers of WTG, main vessel particulars, vessel deck layout and forward speed with significant wave height. Unfortunately, SGRE cannot create a motion analysis in-house, and it hence has to be outsourced due to software and knowledge.

When a motion analysis is not available, DNVGL-ST-N001 has provided default motion criteria depending on the methodology adopted. The first alternative method is the ASD/WSD is design condition where the loading is dominated by environment and storm based on ten years or 50 year return period. According to [DNVGL-ST-N001, Sec. 11.7.2], and it is used to determine the rolling and pitch amplitudes with the heave accelerations for different weather cases and vessel types.

The second alternative method is the LRFD. According to [DNVGL-ST-N001, Table 11-2], it can be used to determine the accelerations in longitudinal, transverse and vertical directions. This method is limit based on with and length of the vessel.

2.4 Vessel grillage

The vessel grillage is where the transport equipment is assembled to the vessel with sea-fasting equipment. The transport equipment is also used as load-spreading to distribute the forces, protecting both transport equipment and vessel hull. There are various methods for sea-fasting of transport equipment as stoppers, pretension chain or corner casting. It must be noted that the transport equipment must be supported in all directions. During sea transporting, the transport equipment and wind turbine components can be subjected to uplift and also need to be lashed. There are two methods for modelling the vessel grillage, depicted in Fig. 2.8.

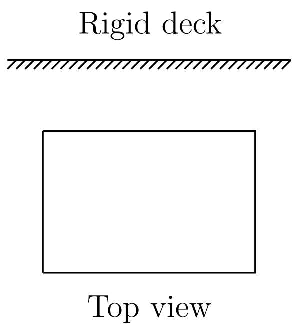

(a) Rigid vessel grillager.

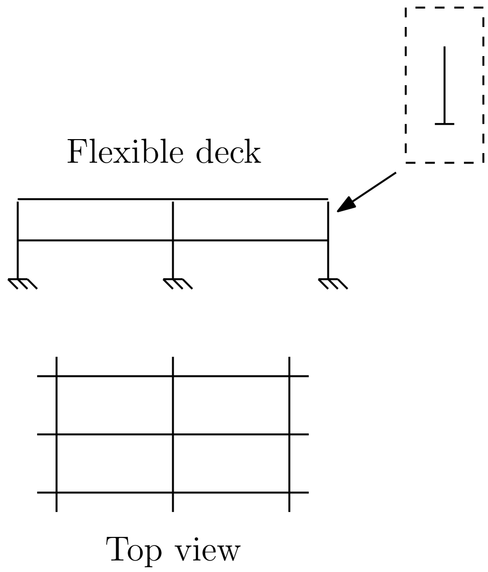

(b) Flexible vessel grillager.

Figure 2.8: An overview of modeling of grillager.

The first methods is the rigid vessel grillage illustrated in Fig. 2.8a and the second methods is flexible grillage illustrated in Fig. 2.8b. The flexible grillage requires data from the vessel used in the marine operations. The modelling of vessel grillage has an effect on the overall stress of the transport frame.

2.5 Marine operation

Only the loaded trip hours are taken into account for the fatigue analysis, shown in Tb. 2.1. The loading in port and sailing back unloaded are not relevant loads for the fatigue analysis. Where the number of cycles is required to determine the fatigue damage, the amount of cycles is calculated based on the amount of time per trip and the wave period.

Table 2.1: Operation profile for installation vessel

Vessel voyage	Time [hr]	Occurrences	Total Time [hr]	Type	Load type
Sailing	12	1	12	Loaded	Transit
Jacking up	3.52	6	21	Loaded	Survival
Installation	30	6	180	Loaded	Survival
Jacking down	1	6	6	Loaded	Survival
Field moves	1	5	5	Loaded	Transit
Sailing back	12	1	12	Unloaded	-
Loading in port	48	1	48	Unloaded	-

2.5.1 Sailing route

The accelerations the transport frame are subjected to depends on the location of the vessel. The sea state changes due to weather, wind, seabed depth, and it impacts the wave height and period, as illustrated in Fig. 2.9.

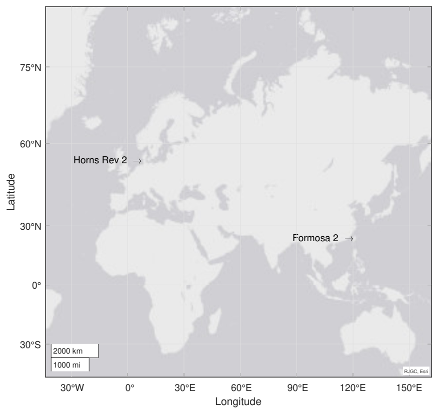

Figure 2.9: An overview over offshore wind farm at Horns rev and Formosa 2.

The transport equipment that is used for the projects at Horns Rev has to be reevaluated based on the new set of accelerations at the offshore project in Formosa 2 in Taiwan [7]. When the sailing route is planned, it is based on the weather and heading.

Chapter 3

Design loads

This chapter introduces the loads during marine operation and its governing loads and forces acting on the structure. The load cases, that are introduces ultimate limit state (ULS) and fatigue limit state (FLS).

3.1 Loads

The loads acting on the transport frame and wind turbine components are the self-weight, sea acceleration, and wind load. The primary loads for transport equipment are the permanent, defined as the gravity acceleration. For environmental loads, is by loads as waves, wind and ice. The load factors necessary for the design phase of transport for the ultimate limit state (ULS) and the fatigue Limit State (FLS) are listed in TB. 3.1.

Table 3.1: Load factor - [A - DNVGL-ST-N001 Sec. 5.9.8.2].

Load factor	Symbol	ULS-a	ULS-b	FLS
Permanent action	γ_G	1.3	1	1
Environmental action	γ_E	0.7	1.3	1

In this master thesis, only the load case for FLS are included in the analysis.

3.1.1 Forces during marine operation

The transport frame on the vessel will experience forces in the three directions, longitudinal, transverse, and vertical, the self-weight and weight of the wind turbine components. As a result, the vessel will have heaves and rolls/pitches simultaneously. When the heave is negative, the vertical accelerations will be deducted. The transport frame is supported by the vessel grillage, where clamps or stoppers is used as sea-fastening equipment. The accelerations generated by the waves are acting in the combined centre of gravity of wind turbine components and the transport frame, depicted in Fig. 3.1.

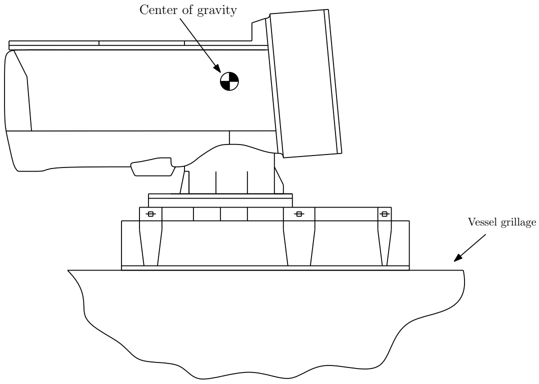

Figure 3.1: Forces action on centre of gravity.

The accelerations at the combined CoG of transport and wind turbine equipment are calculated based on the fixed global vessel coordinate system, presented in Section 2.1. In addition, a simplified approved is presented in Appendix C based on the theory of motion analysis for rolling accelerations.

3.1.2 Descriptions of waves

The fatigue damage is depending on the sea state, where the marine operating is performed. The wave parameters that is necessary is the wave period, where the vessel accelerations are based on the wave height and speed. The regular wave of the definitions and symbols are depicted in Fig. 3.2. There is various way to measuring the wave data by radar or satellite and for a stationary system by wave rider buoy can be used [8].

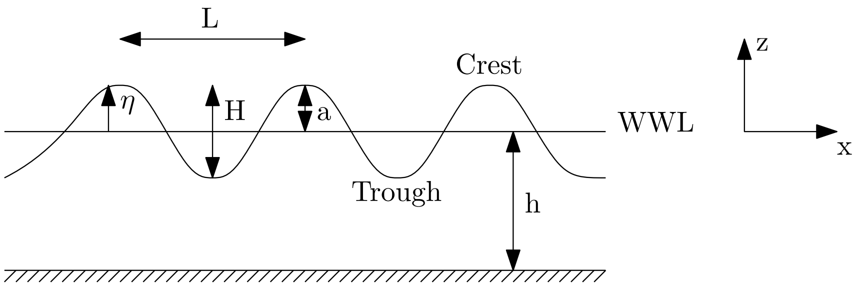

Figure 3.2: Wave definitions and symbols.

When the vessel is operating in the open sea, the growing wind will introduce energy into the wave, increasing height and length. As a result, wind-generated waves are characterized by a highly irregular surface, illustrated in Fig. 3.3.

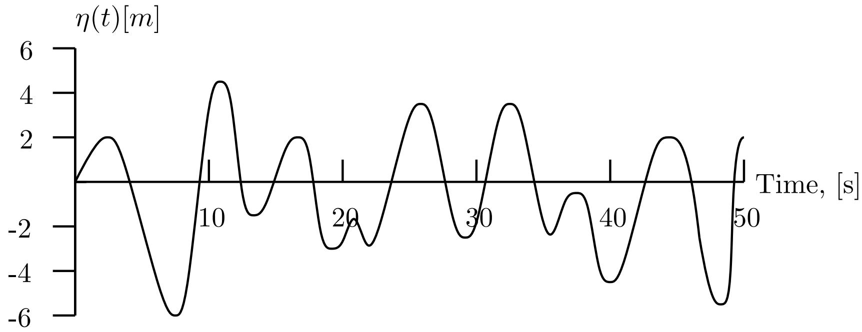

Figure 3.3: Irregular waves.

The irregular wave is with smaller and larger waves in between each other, illustrated in Fig. 3.4. The zero down crossing method can is used to define each wave, where the individual waves are ranked by wave height. The wave can be described in the time domain or frequency domain.

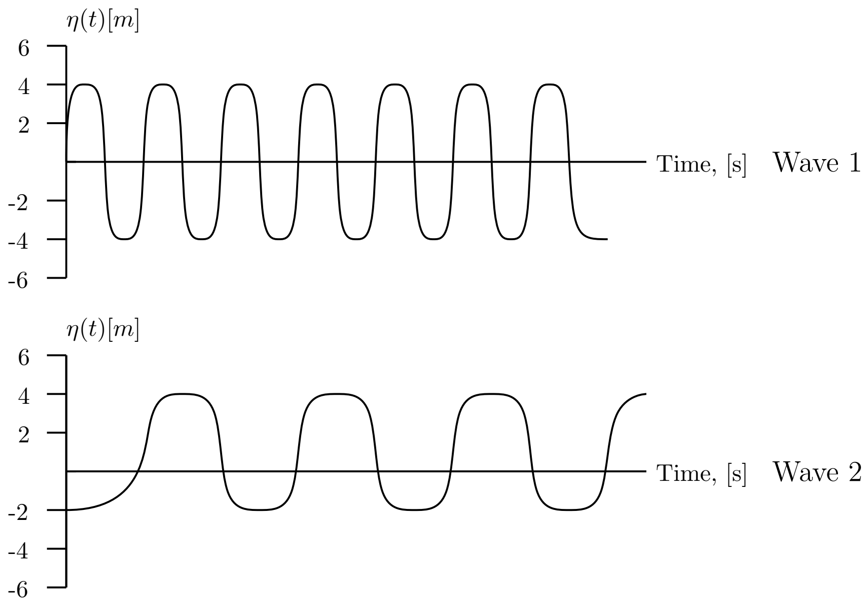

Figure 3.4: Wave 1 and wave 2.

The scatter diagram summarises the wave by representing the joint probability of the wave height and period. The significant Wave (Hs) is the average of the third highest waves.

Table 3.2: Example - Wave scatter data.

Mean Hs [m]	0 [deg]	45 [deg]	90 [deg]	135 [deg]	180 [deg]
1	6.05%	18.15%	18.15%	12.10%	6.05%
1.25	2.92%	8.67%	8.67%	5.84%	2.92%
1.50	0.18%	2.42%	2.42%	1.61%	0.18%
1.75	0.04%	0.55%	0.55%	0.37%	0.04%
2	0.01%	0.02%	0.02%	0.01%	0.01%
Sum of exposed	10%	30%	30%	20%	10%

The wave surface profile at a specific site is unpredictable due to ocean wave trains display random behaviour. The wave scatters diagram provides the occurrence probability of each sea state in a specified ocean site. The main concern with the deterministic method of calculating fatigue is that not all waves have the same period. Also, the stochastic nature of the environment is not really taken into account by assuming all waves are regular. The wave scatters data is used for more precise fatigue estimating, mainly for installations projects, where the shape parameter in Weibull can be determined. This is not further elaborated in this report.

3.1.3 Wind load

The wind load acting on the surface of the wind turbine components and members of the transport are included in the structural and fatigue verification. For fatigue analysis, the wind load in fatigue estimating is only included in marine operations with Windcarrier. The reason is the wind turbine components are exposed to wind, and the wind direction is assumed to be always in line with the governing wave direction. The shape coefficient is determined for each member and wind turbine components, according to [C - DNV-RP-C205, Sec. 5.4]. The centre of action point (CoA) for the wind load is defined as the centre of the transport frame with wind turbine components. However, the aerodynamic sheet must be used to determine the wind load for the blades, and the data is confidential. The wind velocity profile in the open sea related to a reference height can be found in Appendix D.

For Windcarrier, the height varies when elevating. The wind load depends on the placement of the transport frame on the vessel and the height of the wind turbine components. The wind data is based on wind scatter data for the specific project listed in Tb. 3.3. The wind speed ranges are with reference to 10 min mean at a specific height above the water surface. The Weibull parameters scale and shape are determined based on the wind data. This data is used in the following calculations for the elevated condition. The accumulated damage due to this wind loading is added to the calculated damage in transit condition.

Table 3.3: Example - Wind speed scatter data.

Wind speed [m/s]	Wind speed [m/s]	Height [m]	Cycles during project
12	14	5%	3.88E+06
10	12	9%	5.17E+06
8	10	12%	6.10E+06
6	8	17%	6.32E+06
4	6	18%	5.65E+06
2	4	19%	4.19E+06
0	2	20%	2.31E+06
-	-	100%	3.36E+07

The wind Wind speed scatters data is used for the elevated condition during installations projects. Notes that the above wind speed (ranges) are with reference to 10 min mean at 10 m above the water surface. The wind data can be used to determine the Weibull parameters scale and shape. This is not further elaborated in this report.

3.2 Load cases

When designing transport equipment, there are several load cases from 10 to 200. The setup changes from sea transport, road transport, lift and storage. It is not always possible to create symmetry construction and then eliminate some load cases. The main load cases are both for ULS-a and ULS-B and FLS according to [A - DNVGL-ST-N001 Sec. 5.9]. The accelerations from the vessel are often combined with wind load, ice and slosh load it depending on the placement on the vessel and environment at the region. The transport frame can be located longitude or transverse on the vessel deck, as presented in Fig. 3.5. It is not always possible to create symmetry construction and then eliminate some load cases.

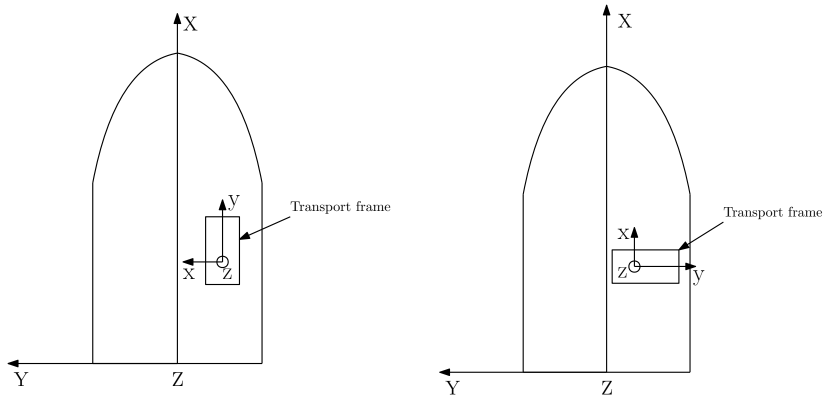

(a) Longitude placement of transport frame.

(b) Transverse placement of transport frame.

Figure 3.5: Overview of placement of transport frame on vessel.

3.2.1 Load combinations

The load combinations for marine operation, according to [A - DNVGL-ST-N001, Sec. 11.6.4], that the transport frame must be evaluated based on the maximum pitch accelerations combined with the minimum and maximum vertical accelerations. The same combination with maximum rolling accelerations. The load cases for quartering sea are combined with 80% of the pitch accelerations and 60% of the rolling accelerations with the minimum and maximum heave accelerations.

For fatigue analysis, the critical connection will be elaborate based on five headings directions will be verified, 0, 45, 90, 135 and 180 deg. For calculation stress range, the following precautions are used for pitch 0 deg vs 180 deg, quartering with 45 deg vs 135 deg, and rolling 90 deg according to [A - DNVGL-ST-N001, Sec. 11.9.15.2].

Table 3.4: Heading directions.

Heading	**0**	**45 vs 315**	**90 vs 270**	**135 vs 225**	**180**	*deg*
Occurrence	10	30	30	20	10	%

Chapter 4

Welded structure

This chapter describe the typical used welding methods in manufacturing of transport equipment. Where the advantages and disadvantages are explained. The definition and symbol are defined and how do weld connection fail.

4.1 Welded connections

The transport equipment used for sea transport, illustrated in Fig. 4.1 is constructed with standardising beams, where plate details are used for stiffness. There is approximately 50 to 300 welded connection, where each load-carrying weld connection is specified with weld types and weld size. The goal for the designer is to identify the weld connection with the highest stresses. The different steel structure members are welded together, where the weld connection transmits the forces from one member to the adjacent member.

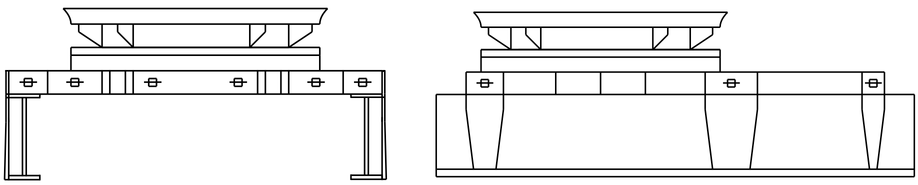

(a) Transport structure front view. **(b)** Transport structure side view.

Figure 4.1: Transport structure used for sea transport.

The welded connections affect the distribution of internal forces and moments and the overall deformation of the structures. In beam software, the weld connection can be modelled as a rigid and pinned connection. The load-carrying weld should be designed to withstand the stress level in the global analysis of the structure.

There are different methods of welding. The first welding process is metal arc welding (MIG), where the weld metal is wire transported out of the welding gun. It makes it easy to weld fillet and groove welds. For TIG welding, it requires that the welder manual add the welding material to the welding process. Before the welded can start, the welder must ensure that the welding procedure specification (WPS) is used during the welding process. The WPS describes the welds quality process based on the requirements for the practical welding work and specifications. The welding process can be done automatically or manually by a certified welder. The welder must set the welding machine with the required energy based on WPS, where it can vary depending on the type of weld.

4.2 Residual stresses in welds

When two members are welded together, the material is exposed to a very high temperature, followed by cooling. In this process, the material is changed due to the heat-affected zone (HAZ). This affect the structure, and it will shrink and deform [9]. Residual stresses are those stresses that remain in the welded connection, leading to welding distortions of the structure, illustrated in Fig. 4.2

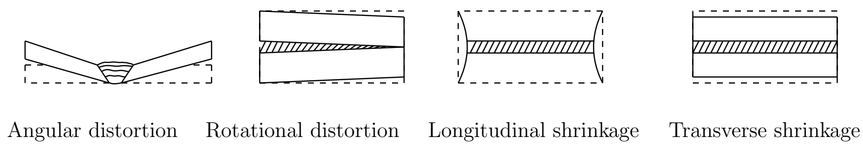

Figure 4.2: Types of welding distortions .

The weld will be left with residual stresses, which are around the yield stress of the material. The effect of the residual stresses can be that it decrease the fatigue strength, but also compressing residual stress can increases the fatigue strength. The residual stress is transmitted to the weld metal and the adjacent base metal. It is complex to include the residual stresses in the fatigue analysis, and this is not further elaborated in this report.

4.3 Weld types

Weld connection is extensively used in the manufacturing of transport equipment. However, the accessibility limits the choice of weld type in the transport frame for welding and inspection. Most weld connections are categories as fillet weld or butt welds, depicted in Fig. 4.3. The base material is melted, and the parts are welded together with weld material [9].

	Weld type	
Joint type	Fillet	Groove
Butt	N.A.	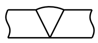
T	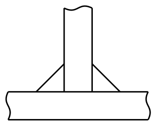	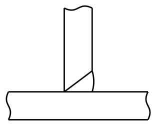

Figure 4.3: Joint types and weld types.

4.3.1 Fillet weld

The fillet weld, illustrated in Fig. 4.4 are two plates joined together. The shape of the fillet weld is approximately triangular. The fillet welds do not require any edge preparation. Therefore, this welding type is simple, fast and economical. The strength of the fillet weld is based on the throat size a.

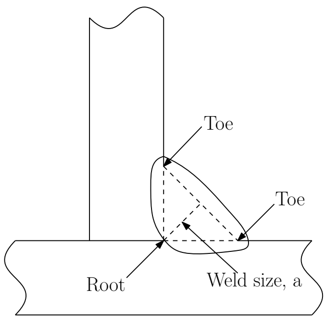

Figure 4.4: Fillet weld definitions and symbols.

The fillet weld can resist load in any direction in compression, shear or tension. However, when using fillet welds for caring shear load, it must be noted that the allowable shear stress is lower than tension or compression strength. When fillet weld is exposed for fatigue loading, they perform poorly due to the stress concentrations at the toe and root.

4.3.2 Groove weld

The T-joint weld, as partial penetration is depicted in Fig. 4.5 are two plates where the butting is against one other and filling the gap between the two contact surfaces with weld metal. It is recommended to used partial penetration welds for strength, where a non-destructive test can verify the quality [10].

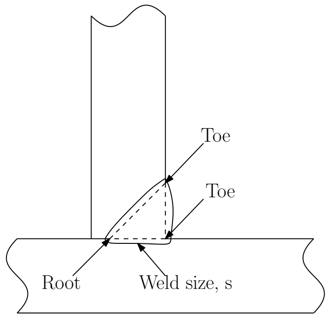

Figure 4.5: Partial weld definitions and symbols.

Under fatigue, the grooving weld does perform better compared to the fillet weld. However, the groove weld is more expensive due to the edge preparation required [9].

4.4 Weld stresses

The load that are transmitted from one member to the adjusted members are based on the the weld connection, is presented in Fig. 4.6.

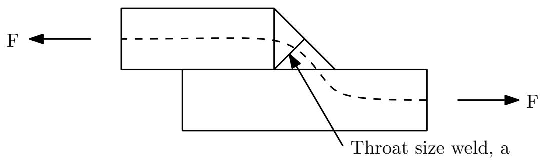

Figure 4.6: Stress flow in welded connection.

The stress is decomposed into normal stress $\sigma_{\perp}$ to weld throat, shear stress $\tau_{\perp}$ acting perpendicular to weld axis and shear stress $\tau_{\parallel}$ parallel to weld axis. The notations for stress components in weld are shown in Fig. 4.7.

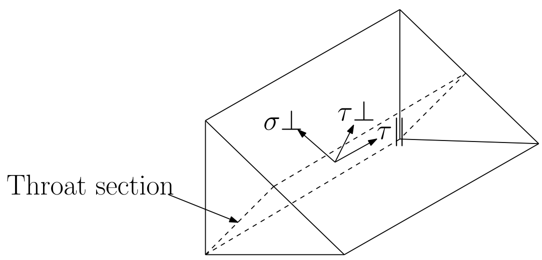

Figure 4.7: Weld definitions and symbols..

The equivalent weld stress is given as [D - DNVGL-OS-C101, Sec. 3.6.7]:

$$\sigma_w = \sqrt{\sigma_\perp^2 + 3 \cdot \left(\tau_\perp^2 + \tau_\parallel^2\right)} \tag{4.1}$$

Before the effective weld stresses can be determined, the three stress components must be evaluated based on the weld properties.

Where the the normal stress $\sigma_\perp$ is given as:

$$\sigma_\perp = \left(\frac{F_z}{a_w} + \frac{M_x}{w_x} + \frac{M_y}{w_y}\right) \cdot \cos(\theta) + \left(\frac{F_x}{a_w} + \frac{M_z}{w_z}\right) \cdot \sin(\theta) \tag{4.2}$$

Where M_x, w_y and w_z is the elastic section modulus and a_w is the arena of the weld throat, which is explained Section 4.5.

The shear stress across weld is given as [D - DNVGL-OS-C101, Sec. 3.6.7]:

$$\tau_\perp = \sigma_\perp \tag{4.3}$$

The shear stress along the weld is given as [D - DNVGL-OS-C101, Sec. 3.6.7]:

$$\tau_\perp = \frac{F_y}{a_w} \tag{4.4}$$

4.5 Weld strength

The strength of the weld connection depends on the weld geometry illustrated in Fig. 4.8. Where the x-axis is transverse, the y-axis is longitudinal, and the z-axis is vertical.

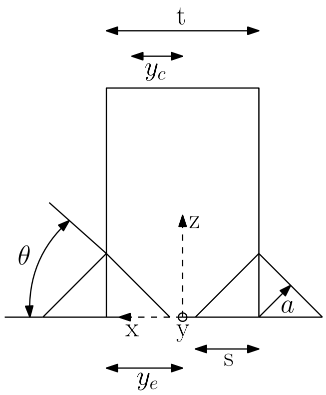

Figure 4.8: Weld geometry.

Where t is the plate thickness, a is throat, s is the penetration of partial weld, and θ is the weld angle. y_e and y_c is the distance determined in Eq. 4.5 and Eq. 4.6.

The distance to center of throat is given as:

$$y_c = \frac{1}{2}\left(t \cdot +a \cdot \cos\theta\right) \tag{4.5}$$

The distance to extreme fibre of throat is given as:

$$y_e = y_c + \frac{1}{2} \cdot a \cdot \cos\theta \tag{4.6}$$

For a double fillet weld, the strength is defined as the cross-section and the section proprieties. The projected weld cross-section is illustrated in Fig. 4.9.

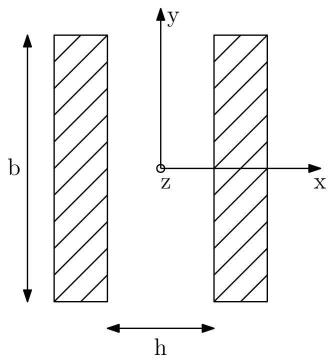

Figure 4.9: Weld cross-section projected.

The first property in strength is the area of the weld, given as:

$$A_w = 2 \cdot a \cdot L_w \tag{4.7}$$

L_w is the weld length, and a is the throat size.

When analysing weld connection based on finite elements stresses, the section properties in the y-axis, x-axis and z-axis are necessary for determining the equation weld stresses. In this case, the elastic theory is used to determine the section properties.

The section modulus in x-direction:

$$W_{el\,x} = \frac{1}{3} \cdot a \cdot L_w^2 \tag{4.8}$$

The section modulus in y-direction:

$$W_{ely} = \frac{2}{y_e} \cdot \left(\frac{1}{12} \cdot l_w \cdot a + l_w \cdot y_c^2 \right) \tag{4.9}$$

y_c is the distance to extreme fibre of throat and y_e is the distance to the center of throat.

The section modulus in z-direction:

$$W_{elz} = \frac{1}{3} \cdot a \cdot L_w^2 \tag{4.10}$$

The weld connection between members does not necessarily, have the same mechanical properties as the base material. The fillet metal used in the welding process can be matched, under-matched or over-matched based on the base metal. When welding two parts with different material strength, the material with lower strength properties shall be used in the design. The strength of the filler metal is in tensile strength.

The strength of the weld connection is determine as [D - DNVGL-OS-C101, Sec. 3.6.7]:

$$\sigma_w \leq \frac{f_u}{\gamma_{MW} \cdot \beta_w} \tag{4.11}$$

The correlation factor β_w is defined based on the steel grade for the lowest ultimate tensile strength [D - DNVGL-OS-C101, Table 4] and γ_{MW} is the material factor for welds [D - DNVGL-OS-C101, Table 1]. For the normal stress perpendicular to the throat the strength is determine as [D - DNVGL-OS-C101, Sec. 3.6.7]:

$$\sigma_\perp \leq \frac{f_u}{\gamma_{MW}} \tag{4.12}$$

4.6 Weld cracks

The failures in welded structures can result in damage, injury and financial loss. The two critical locations for a fillet weld is at the root and the toe, illustrated in Fig. 4.10. The toe crack is a crack that grows through the base plate. The root crack is failures inside and grows through the cross-section of the weld. Root cracks are hard to detect and monitor during the inspection of the structure.

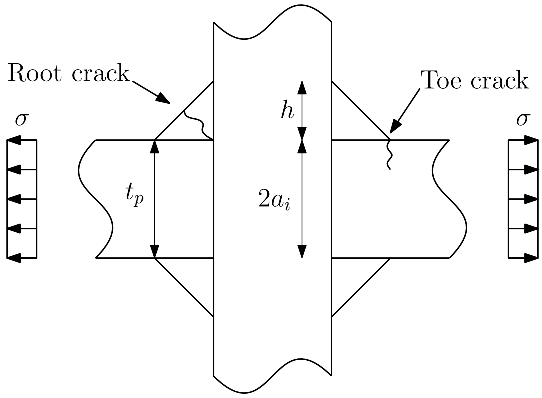

Figure 4.10: Toe and root crack.

It is recommended that the weld connections are designed to minimise the probability of root cracks for ensuring sufficient strength of the root from failure. This is done by the use of partial penetration welds or fully penetrate welds [B - DNVGL-RP-C203, Sec. 2.8].

When using the penetration welds, there is no root and no cracking in the root area. The fabricating cost is higher due to the preparation of plate edges for welding. The guideline for [B - DNVGL-RP-C203, Figure. 2-15] are depicted in Fig. 4.11. The diagram shows the minimum penetration needed to minimise the probability of root failure.

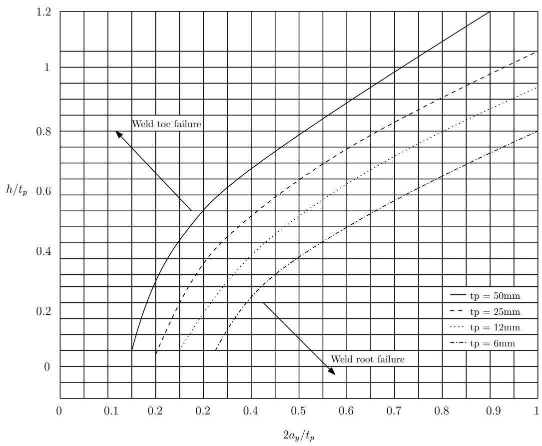

Figure 4.11: Weld geometry with probability of root failure equal toe failure [B - DNVGL-RP-C203, Sec. 2.8].

Where t_p is the thickness of the plate, a_i is the distance between fillet welds, and h is the weld leg length.

Chapter 5

Fatigue of welded connections

This chapter describes the background theory for fatigue analysing and review the most used fatigue methods. An offshore structures primary failure is fatigue failure due to exposed cyclic loading from sea accelerations. The fatigue damage is local, and it makes fatigue analysis complex due to many factors such as fatigue assessment, geometrical, environment, and imperfection.

5.1 General

For offshore structures, the stress response from the waves is typically 5 million cycles a year. It is recommended to use a high cycles region for the fatigue analysis.

The three main types of fatigue analysis used in practice are fracture mechanics, stress or strain. For offshore structures, fatigue is stress-based, but fracture mechanics can be used as a complement to verify the remaining life after a crack is discovered during the inspection of the structure.

The fracture mechanics is defined by the crack length, where the parameters used for defined the resistances is the crack growth rate and the stress intensity factor. The crack growth is an estimate based on the Pariss law, where the parameters needed to determine when the failure occurs the initial crack length and critical crack length. This is not further elaborated in this report.

The loads are through various operating during voyaging as rolling, pitching and yaw motions. This repetitive process can develop stresses that lead to crack growth and result in progressive and localised structural damage. Fatigue damage can develop in regions like welding, where there is a stress concentration due to the geometry change.

5.2 Fatigue loading

The cyclic loading from the vessel motions is due to the dynamic response from the wave actions. This means that the stress state of a structure is alternating between two or multiple states. For example, a simple alternating stress state following a harmonic function and with variable amplitude is illustrated in Fig. 5.1.

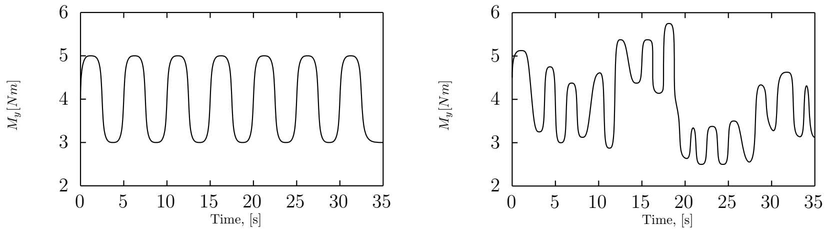

(a) Constant amplitude.

(b) Variable amplitude.

Figure 5.1: An overview of the main components in a typical blade rack.

5.2.1 Fatigue stress

The fatigue stress range defined the allowed numbers of cycles. The stress and time curve is illustrated in Fig. 5.2, where the fatigue stress may be given either in terms of ranges or amplitudes.

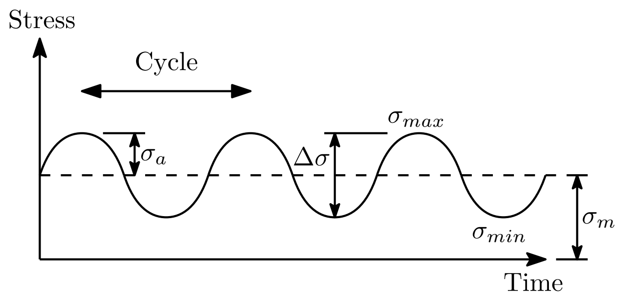

Figure 5.2: Stress related notation.

The stress has a mean stress σ_m, a stress amplitude σ_a and a stress range Δ_σ. The parameter that affects the fatigue damage is the stress amplitude. However, the mean stress must be taken into account as well. If the mean stress is compression, it allows for higher stress amplitudes, which comprises mean tensile stress, which increases the sensitivity to fatigue damage. The stress range is determined as the difference between the minimum and maximum stress in a cycle as:

$$\Delta\sigma = \sigma_{max} - \sigma_{min} = 2 \cdot \sigma_a \tag{5.1}$$

5.3 Fatigue strength

For high cycle fatigue, the fatigue strength is expressed based on an S-N curve. The fatigue test is obtained from specimens subjected to bending and axial loads. The S-N curve shows how many cycles an object or weld location can tolerate when subjected to a certain stress range. The stress ranges in the specimens are plotted against the number of cycles to failure (N). The relationship between the stress ranges to a given detail class and the number of cycles to failure, depicted in Fig. 5.3. The numbers of cycles are plotted logarithmic scale.

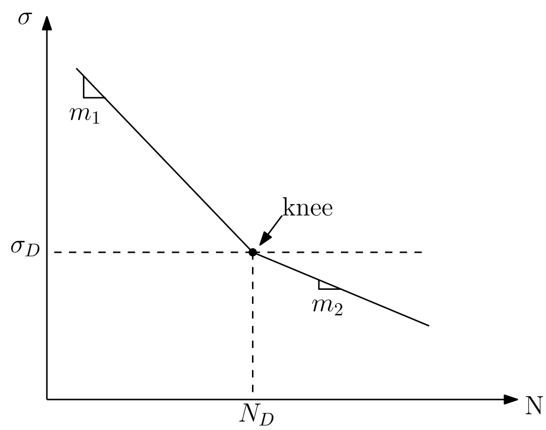

Figure 5.3: S-N curve definitions and symbols.

The knee point is located at some specified number of cycle, typically after which the slope changes. The value (m) is called the slope. However, it is the negative slope. The S-N Curve is based on environment, detail category and plate thickness. The environment and detail category determine which S-N curve is used, while plate thickness corrects the standard S-N curves for the thickness effects. For example, the environment parameter is always air shown in Fig. 5.4, because the transport equipment is on the deck and does not normally come into continuous contact with water.

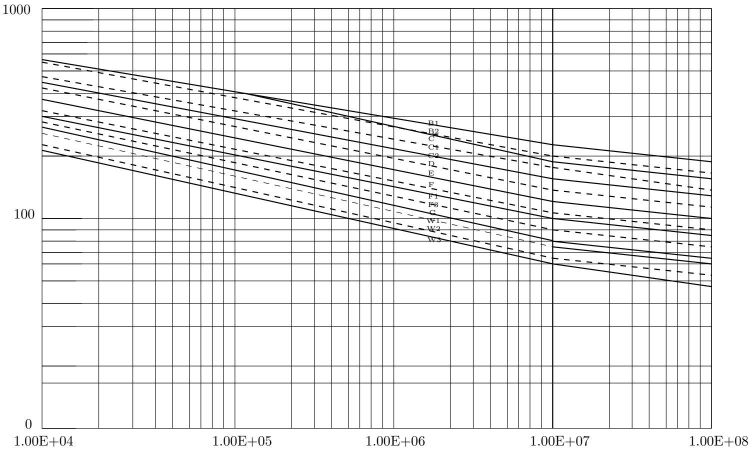

Figure 5.4: S-N curve [B - DNVGL-RP-C203, Figure 2-8].

The letters in the S-N curve define the classification of the structural details and can be found in [B - DNVGL-RP-C203, Appendix A].

5.3.1 Thickness

The plate thickness affects the fatigue damage and S-N curve. Because of this effect, a correction to the standard S-N curves is applied to lower the line in the S-N curve. If the thickness is below a certain reference value, this reference value is used instead of the real thickness, resulting in a correction factor equal to one. The reference value is 25 mm for plate connections according to [B - DNVGL-RP-C203, Sec. 2.4.3]. The thickness modification of S-N curve is calculated as:

$$\log N = \log \bar{a} - m \cdot \log \left(\Delta\sigma \left(\frac{t}{t_{ref}} \right)^k \right) \tag{5.2}$$

Where t_{ref} is the reference thickness for the joint, t is the thickness through the crack, and k thickness exponent on fatigue strength given in [B - DNVGL-RP-C203, Sec. 2.4.3]. Control if the ratio in Eq. 5.3 it should always be more than or equal to one, so t defaults to t_{ref} for $t < t_{ref}$.

$$t_{ratio} = \frac{t}{t_{ref}} \tag{5.3}$$

Two plates with different thickness subjected to bending, depicted in Fig. 5.5. The thick items have more defects as they are difficult to produce to have a completely homogenise structure.

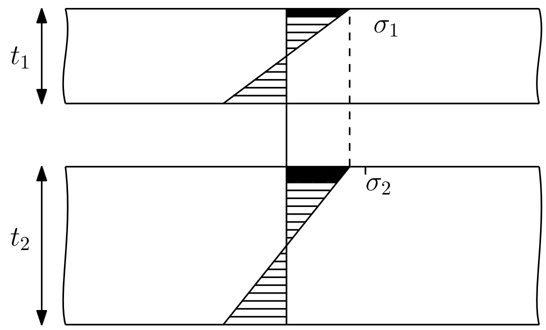

Figure 5.5: Thickness effect.

The thick plate will have a higher stress volume of the material compared to the thin plate. It has been shown that a thick plate has shorter fatigue life than a thick plate subjected to the same bending stress at the surface.

5.4 Fatigue damage

The governing equation used in fatigue damage assessment is the Palmgren-Miner rule, which defines the linear damage as:

$$D = \frac{n_1}{N_1} + \frac{n_2}{N_2} + ... + \frac{n_i}{N_i} = \sum_{i=1}^{n} \frac{n_i}{N_i} \leq 1 \tag{5.4}$$

The stress cycles of a specific stress range are n_i, where $\Delta\sigma_i$, expected throughout the structures life, whereas N_i are the respective cycles to failure under constant amplitude loading and are derived directly from the SN-curve.

The partial damage from each stress cycle can be added, such that the accumulated damage is given as:

$$D = \sum D_i = \sum_{i=1}^{n_{cycles}} \frac{1}{N_i} \tag{5.5}$$

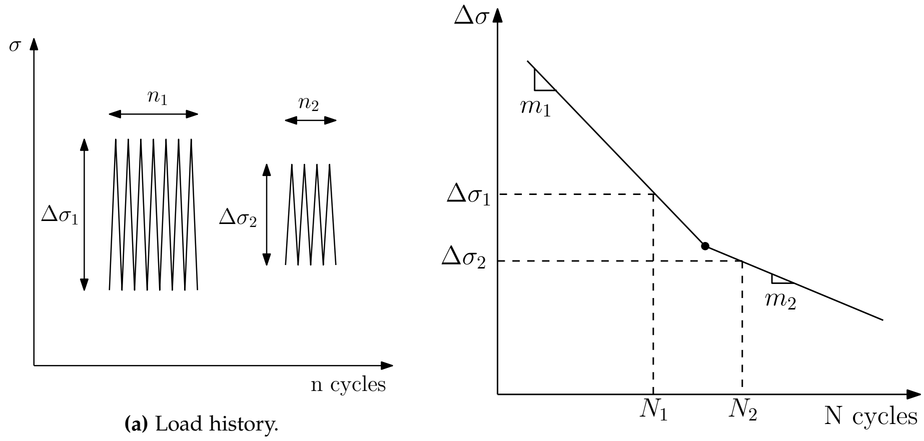

(a) Load history.

(b) S-N curve.

Figure 5.6: Loading bins used for damage accumulation.

For each bin, a partial damage D contributes to the structure, for the total damage is the sum of all partial damage. Therefore, if the total damage is equal to one, the detail is failing. Design fatigue factors (DFFs) may be applied to increase the required design life or to decrease the permissible damage.

5.5 Simplified fatigue assessment

The simplified fatigue assessment method is used to estimating fatigue damage based on long-term stress range distribution. For sea transport, a two-parameter Weibull distribution is commonly used. The assumption is that a probability distribution can accurately express the long-term distribution of stress ranges. Where the fatigue strength is based on the S-N curve and Palmgren-miner rule for damage determination. The method requires few steps, the two parameters Weibull distribution given as [B - DNVGL-RP-C203, Eq. 5.1.1]:

$$Q(\Delta\sigma) = \exp\left[-\left(\frac{\Delta\sigma}{q}\right)^h\right] \tag{5.6}$$

Q is the probability of exceeding the stress range $\Delta\sigma$, h is the Weibull shape parameter, and q is the Weibull scale parameter, defined based om the stress range. The stress range is described by two-parameters Weibull distribution illustrated in Fig. 5.7. Where h is the shape parameter and q is the scale parameter.

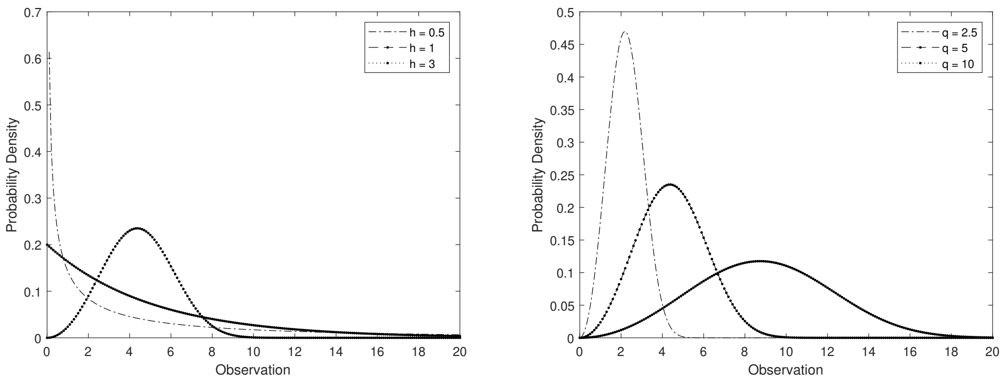

(a) With constant scale parameter q=5. **(b)** With constant shape parameter h=5..

Figure 5.7: Two-parameters Weibull distribution.

Fig. 5.7a the scale parameter specifies the magnitude of the stress ranges, stretching the distribution. In Fig. 5.7b the shape parameter affects the shape of the distribution and not shifting or stretching it.

The Weibull scale parameter is given as in [B - DNVGL-RP-C203, Eq. 5.1.2] defined in in Eq. 5.7:

$$q = \frac{\Delta\sigma_0}{(\ln n_0)^{1/h}} \tag{5.7}$$

$\Delta\sigma$ is the largest stress range in n_0, and it is the total number of cycles, and h is the Weibull shape factor. Where the damage is determined for single-slope S-N curve [B - DNVGL-RP-C203 Eq. 5.1.3]:

$$D = \frac{v_0 \cdot T_d}{\bar{A}} \cdot q^m \Gamma\left(1 + \frac{m}{h}\right) \leq \eta \tag{5.8}$$

Where T_d is the design life in seconds, v_0 is the average zero up-crossing frequency. $\bar{A}$ is the interception of the N-axis and m is the inverse slope of the S-N curve. The S-N curve parameters describe the fatigue strength and dependent on the stress direction and weld detail.

For a system with two processes is presented, as in marine operation as rolling and pitching, the combined fatigue damage can be determined as [B - DNVGL-RP-C203, Eq. D.3-1]:

$$D = D_1 \cdot \left(1 - \frac{v_2}{v_1}\right) + v_2 \cdot \left(\left(\frac{D_1}{v_1}\right)^{\frac{1}{m}} + \left(\frac{D_2}{v_2}\right)^{\frac{1}{m}}\right)^m \tag{5.9}$$

Where the damage is determined for two segment S-N curve:

$$D = \frac{v_0 \cdot T_d}{\bar{A}} \cdot q^m \Gamma \left((1 + \frac{m}{h} \right) \leq \eta \tag{5.10}$$

The shape parameter can be determined by fitting a two-parameter Weibull distribution to the measured stress ranges. In the case where there are no measurements, the shape parameter can be determined based on different options. The shape parameter can be determined according to [E - DNVGL-CN-30.7, Sec. 4.3]:

$$h_0 = 2.21 - 0.52 \cdot \log_{100}(L) \tag{5.11}$$

Where L is the vessel length between perpendiculars, when using this method for determining the shape parameters, requires knowledge regarding the vessel length.

Chapter 6

Fatigue assessment

This chapter describes the most partial method used for fatigue assessment in the industry. The stress range is a governing parameters in fatigue, and the methods used for assessment are based on the nominal-, the structure stress, equivalent weld stress and notch stress.

6.1 Weld stresses

Different types of fatigue assessment approaches have been developed for welded connections. The reason is that welded connections are exposed to fatigue damage, where the stress is defined by three components are depicted in Fig. 6.1.

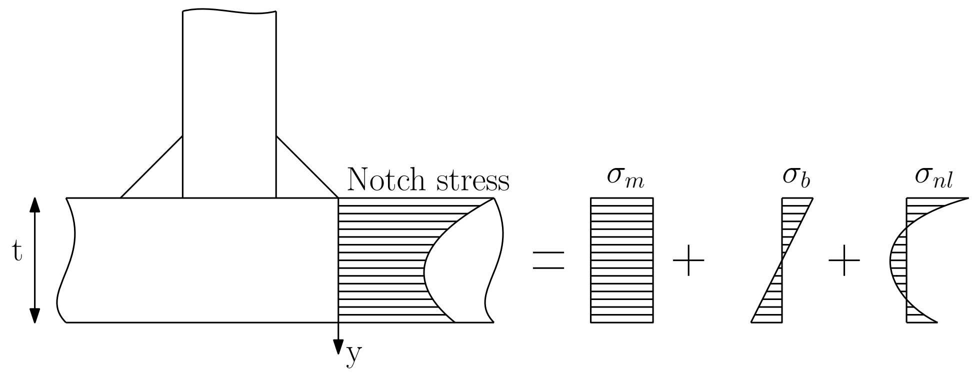

Figure 6.1: Stress distribution for various stress components at weld toe.

Where σ_m is the linear membrane stress, which is constant over thickness. The bending σ_b, which vary linearly over the thickness. σ_{nl} is the non-linear stress distribution, [G - IIW-2259-15, Sec. 2.2].

The membrane stress σ_m is given as:

$$\sigma_m = \frac{1}{t}\int_0^t \sigma_y dy \tag{6.1}$$

The bending stress σ_b is given as:

$$\sigma_b = \frac{6}{t^2}\int_0^t (\sigma_z - \sigma_m)\left(\frac{t}{2} - y\right) dy \tag{6.2}$$

The non-linear stress σ_{npl} is given as:

$$\sigma_{nl}(z) = \sigma_y - \sigma_m - \left(1 - \frac{2 \cdot y}{t}\right)\sigma_b \tag{6.3}$$

The structural stress σ_s is defined as the membrane and bending parts:

$$\sigma_s = \sigma_m + \sigma_b \tag{6.4}$$

The concept behind hot spot stress is to exclude the non-linear part of the local stress due to unknown parameters such as the weld toe radius. The hot spot stress includes the macro-geometric stress concentrations due to the weld geometry.

6.2 Nominal stress

The nominal stress is determined based on the load applied to a sectional area. It can be used for the fatigue assessment of standardised welded connections. This method is straightforward, assuming using the weld stress is equal to the stress far-way from the weld connections. The stress is based on the loads and the sectional properties of the weld or members. However, in finite element, only the bending and membrane stress is used in determining nominal stress. The S-N curve used with the nominal stress is recommended to be use with the appropriate with the classification of the structural details, which can found in [B - DNVGL-RP-C203, Appendix A]. The nominal stresses is determined analytical by Naviers equation given in Eq. 6.5:

$$\sigma_n = \frac{F}{A} + \frac{M}{I} \cdot y \tag{6.5}$$

F is the axial force, A is the cross-section area, M is the bending moment, I is the moment of inertia of the cross-section, and y is the distance from the centroid to the point considered. Therefore, before the nominal stress can be used is must be determined for both maximum and minimum loading in order to calculated the stress range $\Delta\sigma_n$.

Using the nominal stress for fatigue analysis, the references used for S-N curves must be based on the nominal stress. However, finding a suitable reference detail is sometimes tricky if the geometry of the connection is not simple. The nominal stress can be determined in the global beam model and used to analyse the estimated fatigue damage. It is easier to change the cross-section of the beam element and then lower the nominal stresses.

6.2.1 Local approaches

The critical area includes weld detail with plated structures. It may be necessary to modify the nominal stress and consider the local stress at the critical location.

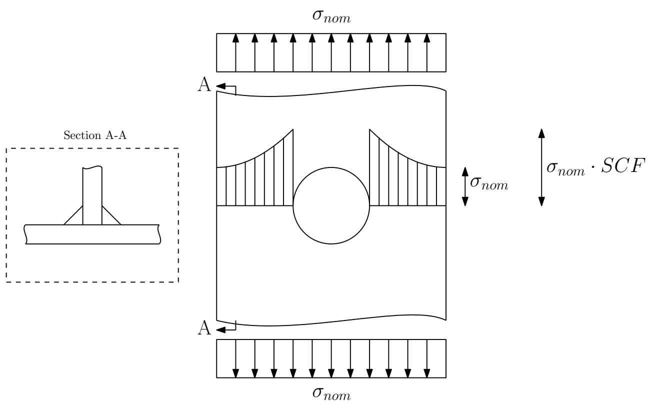

Figure 6.2: Nominal stress - Local stress with stress concentration factor.

The first method for plated structures is to use the nominal stress, where a stress concentration factor is needed to account for the geometry change. This is expressed in Eq. 6.6, according to [B - DNVGL-RP-C203, Sec. 2.3.2].

$$\sigma_{local} = \sigma_{nom} \cdot SCF \tag{6.6}$$

The other method according to [B - DNVGL-RP-C203, Sec. 2.3.3], is to use the hot spot S-N curve with the nominal stress. However, the relation between nominal stress and hot spot stress given in Eq. 6.7:

$$\sigma_{hot} = \sigma_{nom} \cdot SCF \tag{6.7}$$

Where the σ_{hot} is the hot spot stress, σ_{non} is the nominal stress and SCF is the structural stress concentration factor.

6.3 Hot spot stress

The hot spot methods are used when there is no clear definition of the nominal stresses. It requires more time for finite element modelling, and the advantage is that it is a more accurate way to analyse the stresses at the weld toe for fatigue analysis. Applying the hot spot methods for transport equipment is only for a small region of the model. This method uses the stresses obtained and extrapolated linearly to the weld toe. In hot spot method the stress concentration is already calculated in the model. Where the S-N curve used with the hot spot stresses is the D-curve presented in Section 5.3. Generally, two stress read-out points are used, located at 0.5t and 1.5t away from the weld toe, illustrated in Fig. 6.3.

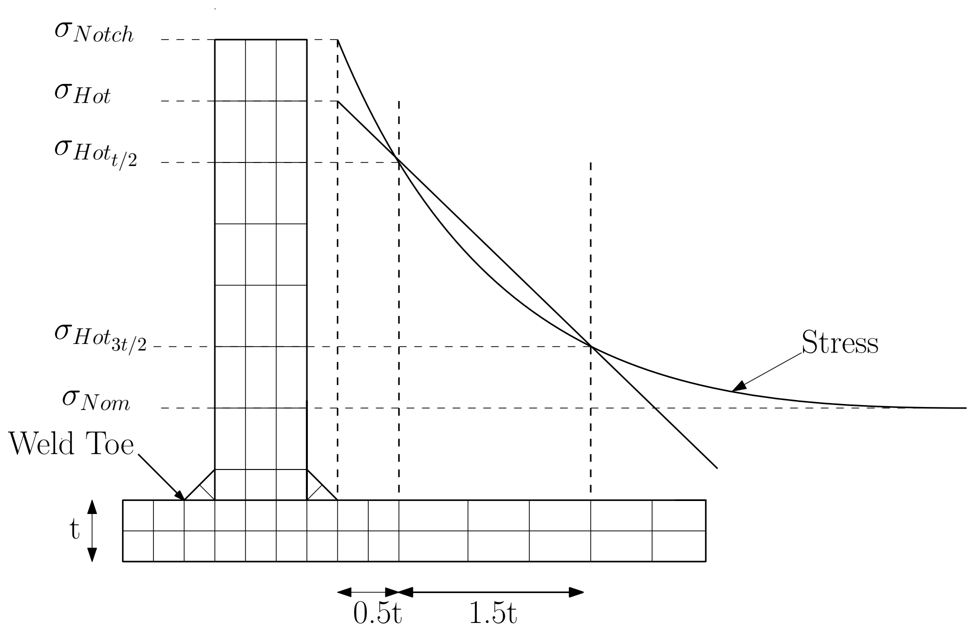

Figure 6.3: Principle of hot spot stress extrapolation - [B - DNVGL-RP-C203, Sec. 4.3.3].

The hot spots stress is determine based on two read out point with used of linear extrapolation given as:

$$\sigma_{0t} = \sigma_{0.5t} + \frac{L_{0t} - L_{0.5t}}{L_{1.5t} - L_{0.5t}} \cdot (\sigma_{1.5t} - \sigma_{0.5t}) \tag{6.8}$$

Where the stress is given as σ_{0t}, $\sigma_{0.5t}$ and $\sigma_{1.5t}$, at distance L_{0t}, L_{0t} and L_{0t}, listed in Tb. 9.8.

For modelling with three-dimensional elements, the elements settings in ANSYS is quadratic it is a higher-order element. The first two or three elements in front of the weld toe are selected to correspond to the plate thickness, the length of the elements should be 2t. When using three-dimensional elements, it is recommended that also the fillet weld geometry is modelled to achieve proper local stiffness. The weld geometry is modelled with no fabrication-related imperfections according to [B - DNVGL-RP-C203, Sec. 4.3.2].

6.4 Effective hot spot stress

The effective hot spot stress can be used with three-dimensional elements or shell elements. When modelling with three-dimension elements, the read-out points is at 0.5t and 1.5t away from the weld toe, as illustrated in Fig. 6.4.

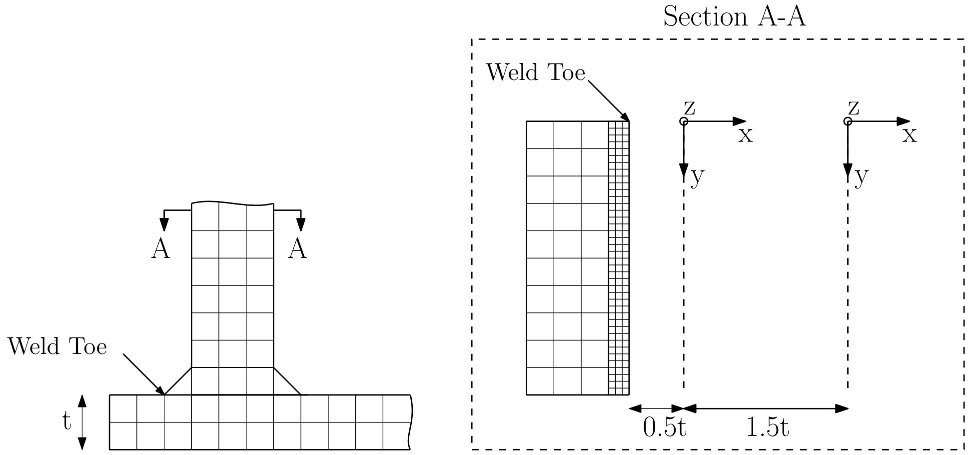

Figure 6.4: Principle of effective hot spot stress method.

The stress is extracted from the surface in ANSYS Workbench, where two path is crated at the two read-out points. The stress that is necessary to determine the principle stress is the stress perpendicular to weld, stress parallel to weld and the shear stress. The effective hot spot stress for method ALT-A is determine according to [B - DNGL-RP-C203, Sec.4.3.4] as:

$$\Delta\sigma_{eff} = max \begin{cases} \sqrt{\Delta\sigma_{\perp}^2 + 0.81 \cdot \Delta\tau_{\parallel}^2} \\ \alpha \cdot |\Delta\sigma_1| \\ \alpha \cdot |\Delta\sigma_1| \end{cases} \tag{6.9}$$

The α value is used to classified how the stress flows compared to weld direction, according to [B - DNGL-RP-C203, Sec.4.3.4]. For $\Delta\sigma_1$ and $\Delta\sigma_2$ is the principle stress determine as in 6.10 and 6.11.

$$\Delta\sigma_1 = \frac{\Delta\sigma_\perp + \Delta\sigma_\parallel}{2} + \frac{1}{2} \cdot \sqrt{\left(\Delta\sigma_\perp - \Delta\sigma_\parallel\right)^2 + 4 \cdot \Delta\tau_\parallel^2} \tag{6.10}$$

The principle stress, $\Delta\sigma_2$ is given as:

$$\Delta\sigma_2 = \frac{\Delta\sigma_\perp + \Delta\sigma_\parallel}{2} - \frac{1}{2} \cdot \sqrt{\left(\Delta\sigma_\perp - \Delta\sigma_\parallel\right)^2 + 4 \cdot \Delta\tau_\parallel^2} \tag{6.11}$$

For method ALT-B according to [B - DNGL-RP-C203, Sec.4.3.4], the read out-point is 0.5t away from the weld toe. The Effective hot spot stress is given as:

$$\Delta\sigma_{eff} = max \begin{cases} 1.12 \cdot \sqrt{\Delta\sigma_\perp^2 + 0.81 \cdot \Delta\tau_\parallel^2} \\ 1.12 \cdot \alpha \cdot |\Delta\sigma_1| \\ 1.12 \cdot \alpha \cdot |\Delta\sigma_1| \end{cases} \tag{6.12}$$

The mesh settings is based on hot spot described in Section 6.3.

6.5 Equivalent weld stress

The equivalent weld stresses is commonly used with ANSYS Workbench to validate the ULS strength for all load-carrying weld connections in the transport equipment. When the transport equipment is modelling in Workbench, all contacts are defined for each member and stiffness combined with a local coordinate system, illustrated in Fig. 6.5.

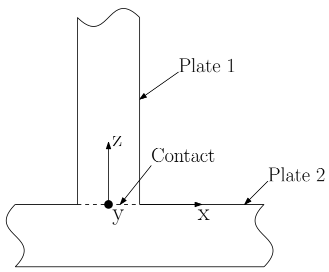

Figure 6.5: Weld contacts in ANSYS Workbench

As shown in the figure, the contact between plate one and plate two are manually defined for each contact in ANSYS Workbench. For each weld connection, the forces and moments are extracted in the x-direction, y-direction and z-direction from ANSYS Workbench illustrated in Fig. 6.6 and copied into Excel.

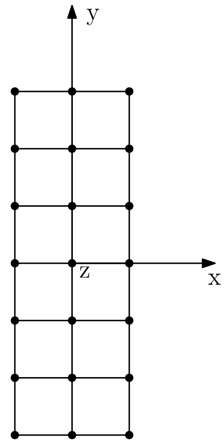

Figure 6.6: Nodal stress in ANSYS Workbench.

The advantage of using the analytical method is when all the weld connection is defined in the Workbench model as contacts, only the load case needs to be changed to FLS and modified the excel sheet for fatigue estimating.

The equation for equivalent weld stresses is given as [B - DNVGL-RP-C203, Sec. 2.3.5]:

$$\sigma_w = \sqrt{\Delta\sigma_{90}^2 + \Delta\tau_0^2 + 0.2 \cdot \Delta\tau_{90}^2} \tag{6.13}$$

When using Eq. 6.13 for determining the weld stress at the weld throat plane, the sections proprieties is explained in Section 4.5. The forces and moments that are extracted to determine the stress components are based on absolute values. This can lead to an over-design welded connection when all values are positive.

6.6 Effective notch stress

Effective notch stress is obtained by prescribing a specific notch geometry. The main idea with the effective notch stress method is to model the weld toe and root with a reference radius. It requires use for finite element and detailed information on the notch geometry in combination with plastic-elastic material models due to local yielding. This method requires high computational time due to demanding mesh requirements and requirements for detailed modelling compared to the nominal and structural hot spot stress method. Therefore, the effective notch stress is not further elaborated in this report. More informations can be found in [B - DNVGL-RP-C203, Ap. D.11].

Chapter 7

Global analyses of transport frame

In the present chapter, the global model imported in Autodesk ROBOT and discretized with 3D beam elements is described throughout this chapter. The geometric representation of the transport frame is described, and next the material parameters of the structure. The purpose of the global model, is to identifies the most governing load cases.

7.1 Introduction

This chapter introduces the global analysis performed in beam software Autodesk robot structural analysis (ROBOT). ROBOT is a structural load analysis software that can verify members based on code compliance. The idea is to unitise ROBOT to screening the equipment for the most governing load cases of the structure and quantify them for fatigue analysis. Although this is normal performed in ANSYS Workbench, in beam software, the structural engineer must take the stiffness of the global model into account.

The process of creating a beam model based on a 3D CAD model is showing in Appendix E. This process can be used with any 3D program as Inventor or SOLID-WORKS. To illustrate this process of creating a beam model, an example based on a transport frame used for the transport of nacelle. In this case, a simple transport frame, depicted in Fig. 7.1. The transport frame is modelled in Autodesk Inventor, where the 3D solid parts in Inventor. The Inventor model is then imported to AutoCAD, where each centre line for each member is defined. The wind turbine components are not included in the global model.

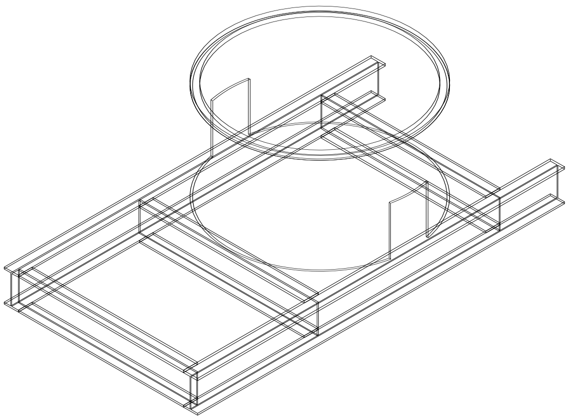

Figure 7.1: 3D model from Inventor in AutoCAD.

The turbine components are model in 3D, which including all details. The input is the CoG and the weight of the wind turbine component. The transport frame is placed transversely as illustrated in Fig. 7.2.

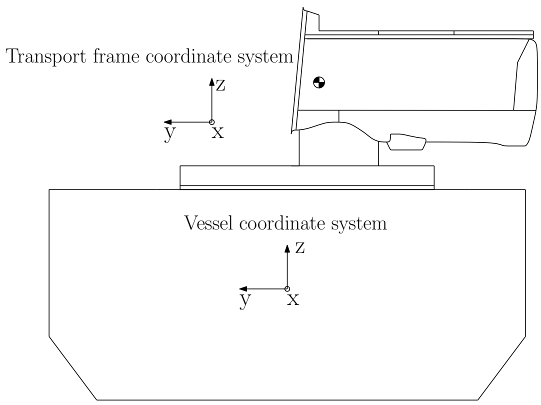

Figure 7.2: Transport frame with nacelle placed transverse on vessel.

However, the interface between the transport frame and the wind turbine component must be verified. To ensure the clamping and the utilisation of the high pretension bolt connections. There must be no damage during transport to the interface of the wind turbine. Otherwise, it will delay the installation, and it has a high cost.

7.2 Structure description

The transport frame consists of HEM600 beams and a 40 mm steel plate barrel with an opening for the door. The HEM600 beam is manufactured according to standards EN 100025-2, and this means the selected beam, in ROBOT, must follow [H - EN 100025-2] to match the overall stiffness of the beam. The global model is defined in AutoCAD based on the Inventor model. The geometry of each member is drawing as a line. The mean frame is depicted in Fig. 7.3, the centre line of each HEM beam has been drawing as a beam element.

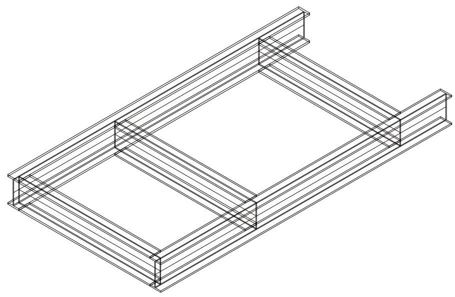

Figure 7.3: The main frame - AutoCAD.

The barrel is a 40 mm steel plate that has been rolled and has a door opening. The barrel is drawing as 12 sides polygon illustrated in Fig. 7.4, representing the barrels overall geometry.

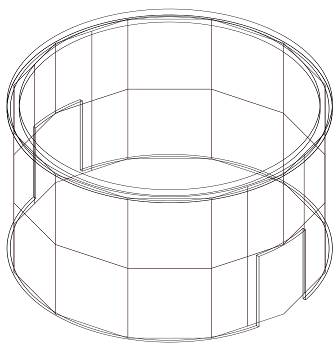

Figure 7.4: The barrel - AutoCAD.

The final global model drawing as beam elements is depicted in Fig. 7.5.

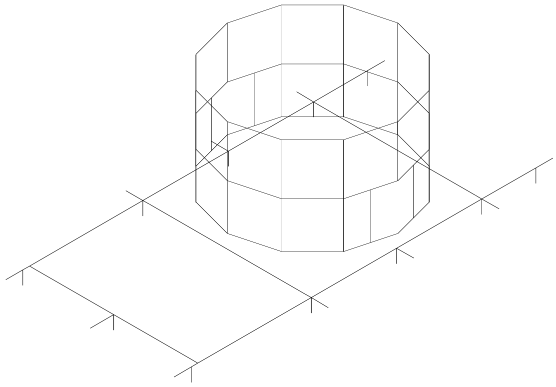

Figure 7.5: The global model - AutoCAD.

The model created in AutoCAD is ready for Autodesk ROBOT.

7.2.1 Cross-section for beam elements

Each beam elements has been defined with a cross-section in ROBOT, as depicted in Fig. 7.6. The main goal is to transmit the load from the CoG of the nacelle through the barrel and to the main frame. The first part is the selected cross-section for the main frame, with HEM600 profiles.

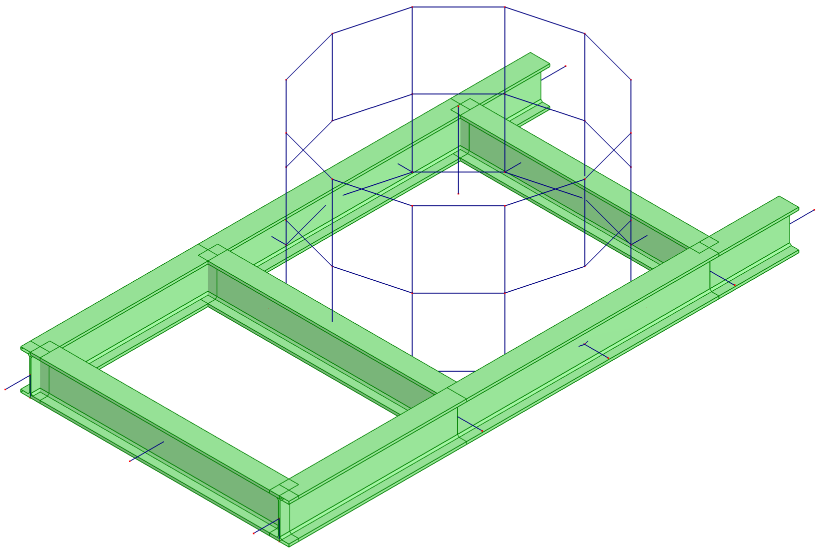

Figure 7.6: The global model main frame with cross-section in ROBOT.

The barrel function in global analyses is the transmit load from the nacelle through the stiffness of the barrel in ROBOT. The cross-section used for the barrel are, depicted in Fig. 7.7. The beam elements for the top flange are defined with a cross-section of solid rectangular with the dimensions length 220 mm and height is 90 mm. The beam element in the centre of the 12 sided polygon has a cross-section as a pipe with a diameter of 4000 mm and thickness of 40 mm. The top part of the barrel is more rigid than the lower part due to the door opening. The cross-section for the 12 sided polygon is a DN400 pipe with a thickness of 10mm. The section modulus of the pipe is equal in all directions. The DN400 pipes are used to transmit the load to the main frame. The DN400 pipe is connected with the main frame, with three-point with each main beam.

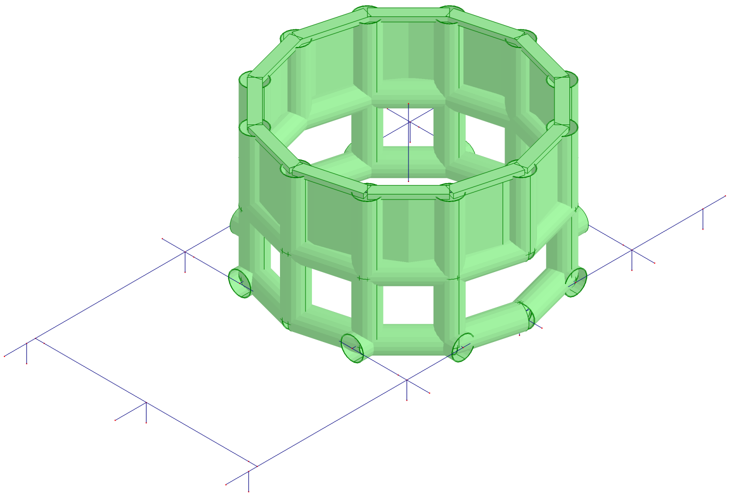

Figure 7.7: The global model barrel with cross-section in ROBOT.

The supports from the sea-fasting are stoppers that support the transport frame in either x-direction or y-direction. The cross-section is solid rectangular with a length of 300 mm, and height is 90 mm and thickness of 25 mm, presented in Fig. 7.8. The beam elements that support the vertical direction are solid rectangular with a height of 310 mm, with 50 mm width and length is 50 mm and thickness of 25 mm.

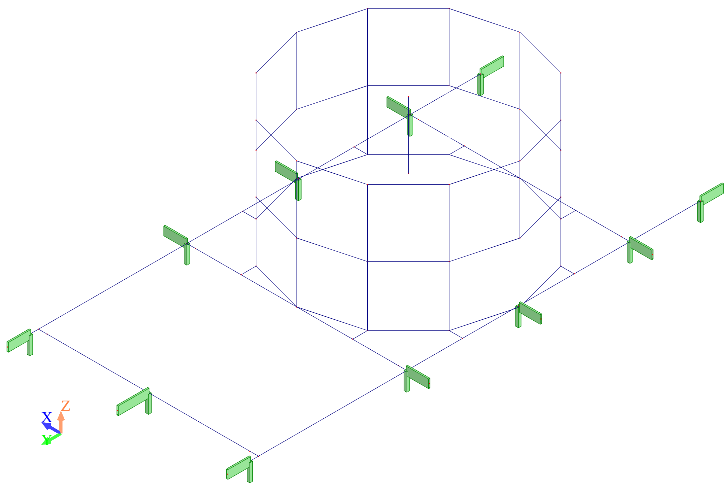

Figure 7.8: The global model stoppers with cross-section in ROBOT.

The global beam element model with cross-section are presented in Fig. 7.9. The next phase in the global model is to set the properties of the material in ROBOT.

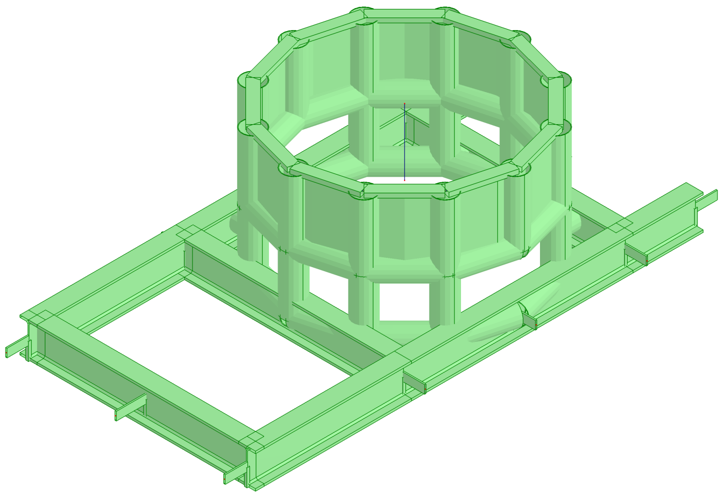

Figure 7.9: The global model with cross-section in ROBOT.

7.2.2 Material properties

The steel used for the transport frame is S355, according to [H - EN10025], while the yield and tensile versus plate thickness are listed in Tb. 7.1.

Table 7.1: Steel properties versus plate thickness.

Properties	Material [MPa]	16<t<40 [mm]	16<t<40 [mm]
Yield	S355	325	345
Tensile	S355	572	589

The material properties in ROBOT is set to linear, based on Hookes Law of elasticity, shown in Appendix F. For linear static analysis, the input the Youngs modulus and Poissons ratio, The mechanical properties used in ROBOT and ANSYS are listed in Tb. 7.2.

Table 7.2: Mechanical properties for all structural steel.

Property	Designation	Value
Youngs modululs	E	210000 MPa
Poissons ratio	V	0.3
Density	ρ	7850 kg/m^3

7.3 Boundary conditions

The vessel deck supports the transport frame, and the stoppers ensure that the transport is supported in all directions. The structure is supported against uplifting during sea transport. The boundary conditions must be chosen to validate the sea-fasting method used during sea transport. The transport frame is supported in all four sides, illustrated in Fig. 7.10.

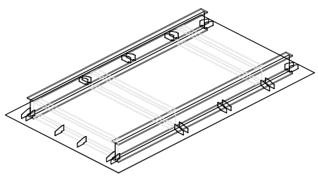

(a) Overview over sea-fasting.

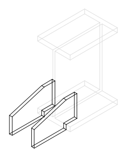

(b) Detail view of sea fasting.

Figure 7.10: Sea-fasting for transport frame during sea.

The supports used in the vertical direction are defined with element type truss, depicted in Fig. 7.11, where the properties are only axis force. This ensures that the moments are transmitted to the stoppers that support in x-direction and y-direction.

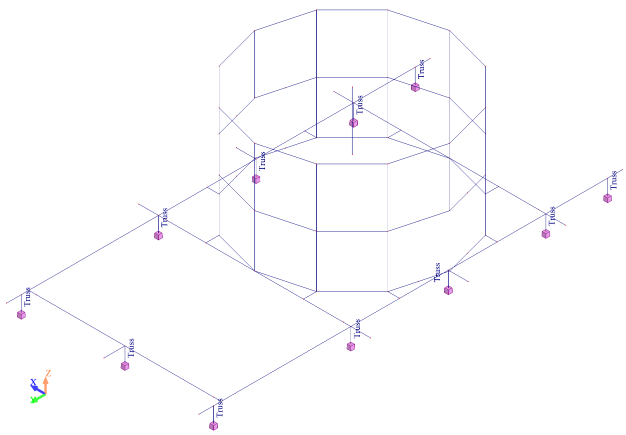

Figure 7.11: Vertical beam elements defined as truss.

The boundary conditions for the vertical truss elements are showing in the figure. This is because the end node of the vertical truss supports is fixed, which is due to rigid motions. The boundary conditions for the supports in x-direction and y-direction are illustrated in Fig. 7.12.

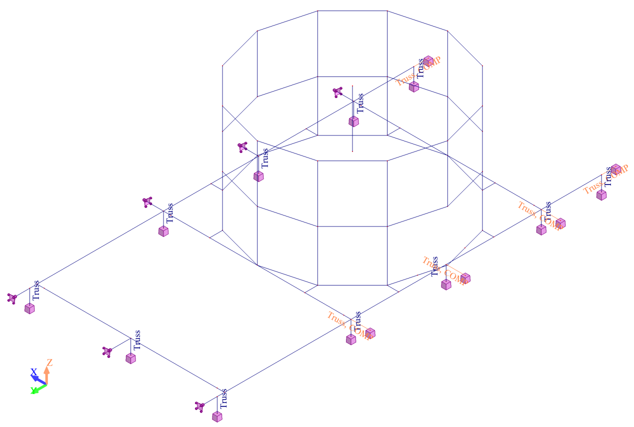

Figure 7.12: Sea-fasting for transport defined with beam elements.

As shown in the figure, when the transport is moving in x-direction or y-direction, the transport frame will be pressed against the stoppers, where the stoppers in the opposite direction will open. This is modelled with a truss that only action under pressure. The moments are transmitted to the stoppers.

7.4 Loads

The loads acting on the transport frame and nacelle is the self-wight and sea acceleration. The first part is to define the input for calculation of scaling factors applied unit load of 1.0 kN. The second part is to the setup of load cases based on unit loads applied scaling factor acting in global x-direction, y-direction and z-direction. Where the load syntax is defined as xx1 = acting in x-direction, xx2 = acting in y-direction, xx3 = acting in z-direction, this is created in Excel, found under virtual files in (Appendix A A.1 - Load-Tool-ROBOT). The load types in ROBOT, is defined as listed in Tb. 7.3.

Table 7.3: Load types in ROBOT.

Case	Load type	List	x	y	z
DL1	Self-weight	Transport frame	1	0	0
DL2	Self-weight	Transport frame	0	1	0
DL3	Self-weight	Transport frame	0	0	1
DL13	Self-weight	Nacelle	0	1	0
LL11	Node force	Master node	1	0	0
LL12	Node force	Master node	0	1	0
LL13	Node force	Master node	0	0	1

The load types in ROBOT is defined as DL for dead-load and LL as live-load. The first three loads are due to the inertia accelerations from motion x-direction, y-direction and x-direction, where it acting on the defined structure properties. The load number 13 is the dead-load for the nacelle in the z-direction. The first important input is the weights of the frame and nacelle, listed in Tb. 7.4.

Table 7.4: Structure loads.

Component	Value [Kg]
Transport frame global	15000
Transport frame drawing	17000
Nacelle	420000

The load factor used in the global ROBOT model is listed in Tb. 7.5. In fatigue analysis, the load factor for the permanent actions and sea accelerations are equal to one. For the weight factor for nacelle γ_{Com} and for transport frame γ_{Frame}, these factors take into account uncertainties in the weight-based on CAD model.

Table 7.5: Load factor - [A - DNVGL-ST-N001 Sec. 5.9.8.2].

Load factor	Sumbol	FLS
Permanent action	γ_G	1
Environmental action	γ_E	1
Weight contingency factor (Component)	γ_{Com}	1.03
Weight contingency factor (Frame structure)	γ_{Frame}	1.10

The global scaling factor on structure self-weight. The global scaling factor is used due to a simplified structure, where detail is missing that increasing the overall weight and loads from the self-weight. The global factor is given as:

$$Global_f = \frac{Weightdrawing}{WeightCADNacelle} \tag{7.1}$$

The load in the z-direction is the self-wights of the transport frame:

$$DL3 = Global_f \cdot transportframe \cdot \gamma_{Frame} \cdot \gamma_G \tag{7.2}$$

The load in the z-direction is the self-wights of the nacelle:

$$DL43 = Nacelle \cdot \gamma_{Com} \cdot \gamma_G \tag{7.3}$$

The vessel accelerations are based on RO/RO transport in the North Sea, between quayside factory and Port of Esbjerg, for nacelle transport. The vessel accelerations are given as roll, pitch and heave are listed in Tb. 7.6.

Table 7.6: Accelerations from motion based on North sea.

Direction	Designation	Value $[m/s^2]$
Longitudinal	Pitch	2
Transverse	Roll	5
Vertical	Heave	3

The accelerations are dived by gravity due to the loads that are applied in ROBOT are unit devices, for longitudinal in the x-axis, transverse in the y-axis and vertical in the z-axis.

$$a_x = \frac{Pitch}{Gravity} = 0.51 \tag{7.4}$$

The inertia accelerations from motion x-direction, y-direction and z-direction for self-weight acting on defined structure properties. The load in x-direction is determine as Eq. 7.5, the same process for load in y-direction and z-direction.

$$DL1 = \gamma_G \cdot \gamma_E \cdot a_x \cdot global_{factor} \cdot x \tag{7.5}$$

The accelerations from the motions acting on the nacelle CoG are defined as live-load. The live-load is in x-direction is determine as Eq. 7.6, the same process for load in y-direction and z-direction.

$$LL11 = Live_{load} \cdot \gamma_E \cdot a_x \cdot x \tag{7.6}$$

7.4.1 Load combinations

The load combinations are generated, as listed in Tb. 7.7. The factor for control of directions and size in ROBOT. The sign or factor will be multiplied with the load factor used to calculate the sea accelerations for each load case. The load combination is scaled based on the load factor.

Table 7.7: Factor for control

No	Description	Ax	Ay	Az
LC-SEA-1	Pos Pitch with + heave	1	0	1
LC-SEA-1	Pos Pitch with - heave	1	0	-1
LC-SEA-2	Neg Pitch with + heave	-1	0	1
LC-SEA-3	Neg Pitch with - heave	-1	0	-1
LC-SEA-4	Pos Roll with + heave	0	1	1
LC-SEA-5	Pos Roll with - heave	0	1	-1
LC-SEA-6	Neg Roll with + heave	0	-1	1
LC-SEA-7	Neg Roll with - heave	0	-1	-1
LC-SEA-8	Pos Quartering with + heave	0.6	0.8	-1
LC-SEA-9	Pos Quartering with - heave	0.6	0.8	-1
LC-SEA-10	Neg Quartering with + heave	-0.6	-0.8	1
LC-SEA-11	Neg Quartering with - heave	-0.6	-0.8	-1

7.5 Results for global analysis

The output from the global analysis is the forces, moments, displacement, reactions forces and stress. The forces and moments in each beam elements are used to validate the cross-section based on Eurocode DS/EN 1993-1. The member design option in ROBOT, are based on buckling in the x-axis and y-axis. The advantage is that the overall strength of the chose cross-section is examined. The load case with the highest deformation is LC-SEA-FLS-5 with rolling as positive and positive heave, presented in Fig. 7.13. The transport frame experiences the largest deformation of approximately 12 mm.

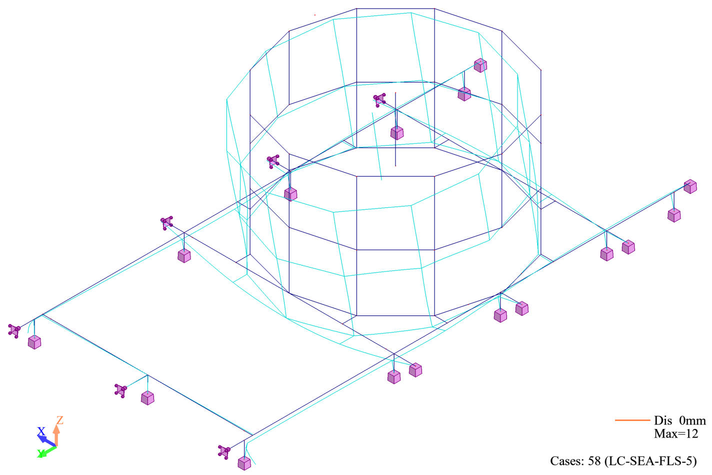

Figure 7.13: Deformation in isometric view (LC-SEA-FLS-5).

The deformation in y-axis and z-axis is presented in Fig. 7.14. It can be seen that the structure is tilting forward, and this creates tension in the front of the frame.

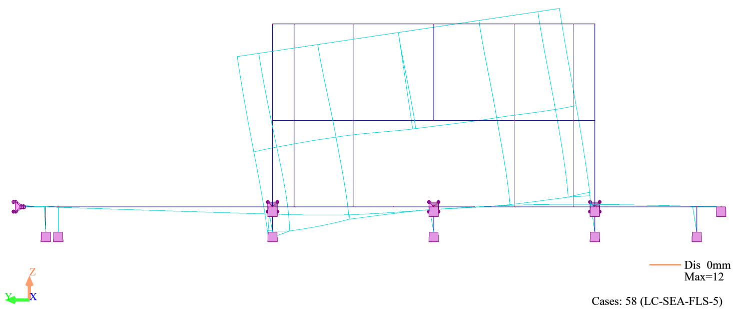

Figure 7.14: Deformation in y-axis and z-axis view (LC-SEA-FLS-5).

This also makes good sense since there is no support under the HEM beam in the global model. The vertical load is moved forward due to the CoG of the nacelle. This makes the global model more conservative, it increases the overall deformation and stress. The reason is that the main frame is not supported in the z-axis.

To determine the stress range, the opposite load case LC-SEA-FLS-7, where the rolling is negative with a negative heave. The deformation of LC-SEA-FLS-7, is presented in Fig. 7.15.

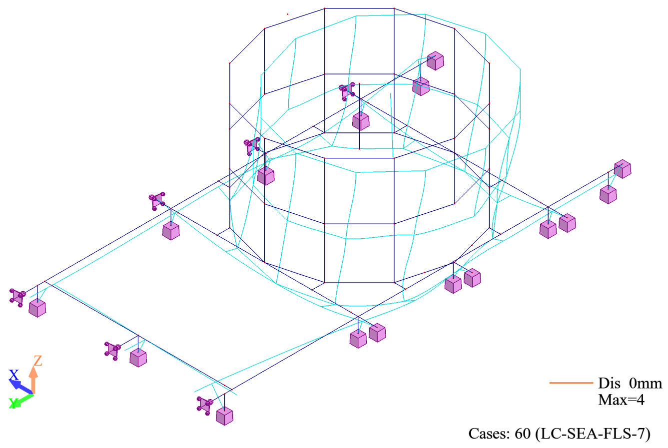

Figure 7.15: Deformation in isometric view (LC-SEA-FLS-7).

In the figure, it can be seen that the transport frame is tilting in the opposite direction due to negative rolling. This allowed the designer to determine the stress range used in fatigue analysis.

7.6 Governing load cases

The governing load case is used to examine the fatigue damage in ANSYS Workbench. The two selected load cases are LC-SEA-FLS-5 positive rolling with a positive heave and LC-SEA-FLS-7 with negative rolling and negative heave.

The results for each member is verification in ROBOT, where each defined section has been calculated based on buckling, where the ratio is given. The highest ratio is 0.61 at member one in Load case LC-Sea-FLS-5, shown in Fig. 7.16.

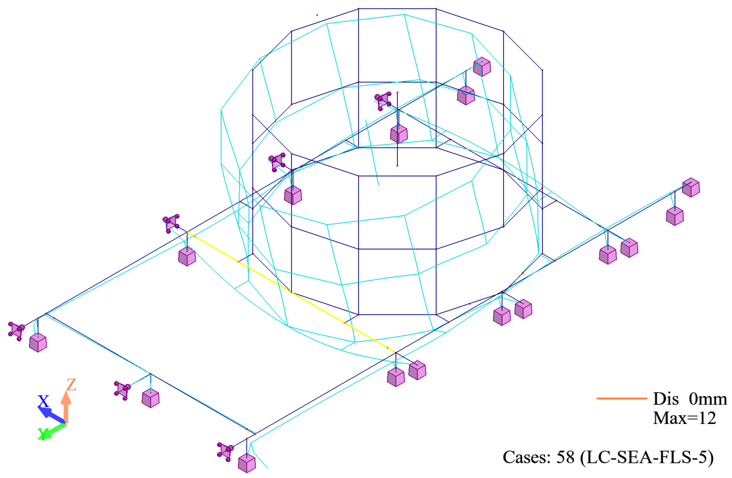

Figure 7.16: Transport frame - highest utility ratio member.

This type of structure is design to handle loads in the vertical direction. As soon the structure is exposed to forces in longitudinal or transverse due to sea accelerations, it becomes weak due to the layout of members.

The reactions forces in all supports for all loads cases are extracted into Excel (Appendix A A.2 - Load-Tool-ANSYS, Sheet - Reaction forces) to examine in which direction the highest reactions forces occur. In this process, it is noted that there no moments in the support. It makes good sense due to the boundary conditions where truss is used that only can absorb the forces in x-direction, y-direction or z-direction. The highest reaction forces are in the y-direction with 1115 kN, and wherein z-direction was 3082 kN based on LC-SEA-FLS-5 load cases.

Chapter 8

ANSYS Workbench analysis

In the present chapter, the worst load case are analysis in ANSYS Workbench to determine the stress range used in fatigue calculation. The ANSYS model is discretized is solid elements are the setup in ANSYS are described throughout this chapter.

8.1 Introduction

The geometry is originally modelled in Inventor as solid parts. The Inventor model is linked to ANSYS Workbench such that a smooth CAD model update is ensured. Based on the original model, two transport frame are modelled, first is model A where the weld connection is not included, and model B is where the weld is included in the model. The two models are presented in Fig. 8.1.

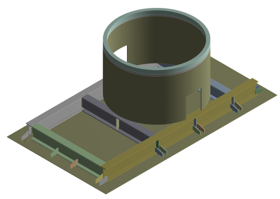

(a) ANSYS model A without weld geometry.

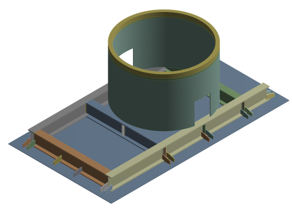

(b) ANSYS model B with weld geometry.

Figure 8.1: An overview of two ANSYS model.

Design changes during the calculation process are created in Autodesk Inventor 2021. The reasons for simplifying the model is to lower the overall elements and nodes in the ANSYS model. For example, the chamfers and fillets will first lower the cross-section of the beams, making it easier to mesh. The following simplifications of the model are listed:

- Rounded corners (chamfers/fillets) are removed.
- Fillets between webs and flanges on I-beams are removed.
- Bolts are removed.

- Lifting accessories and other members not subject to sea loads are removed.
- A dummy of the nacelle flange is added for load application

The ANSYS model is used to calculate the fatigue damage for different fatigue assessment methods based on the governing load case LC-SEA-FLS-5 positive rolling with a positive heave and LC-SEA-FLS-7, with negative rolling and with a negative heave, defined in Section 7.6.

8.2 Mesh

The model has meshed with solid elements (SOLID186), which is a higher-order hexahedral 20 node element. Special attention has been paid to element quality and aspect ratio. The mesh settings are listed in Tb. 8.1

Table 8.1: Mesh settings - ANSYS.

Model	Part	Element type	Method / sizing	Setting
Transport frame	HEM600	Hexa	MultiZone / 50mm	Quadratic
Transport frame	Barrel	Hexa	MultiZone / 100mm	Quadratic
Transport frame	Flange	Hexa	MultiZone / 100mm	Quadratic
Transport frame	Stoppers	Hexa	MultiZone / 20mm	Quadratic
Transport frame	Welds	Quad	Hex dominate/ 10mm	Quadratic
Vessel	deck	Hexa	MultiZone / 100mm	Quadratic
Nacelle dummy	Flange	Hexa	MultiZone / 100mm	Quadratic

The mesh density is of the transport model B with a weld is presented in Fig. 8.2.

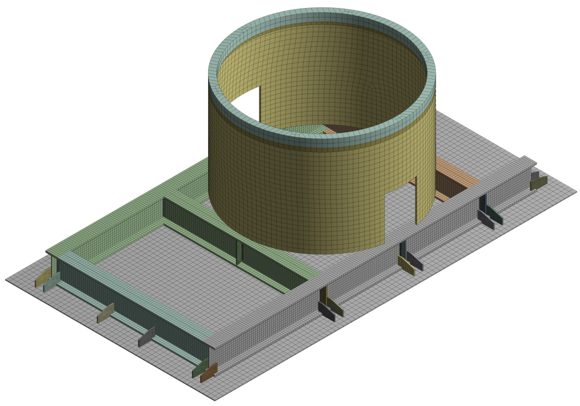

Figure 8.2: Mesh density of model B with weld geometry.

8.3 Contacts

The contacts between the different structural components must be modelled as realistic as possible. Where the contact settings, depending on the functionality of the contact interface. All contacts of the transport frame are manually defined in ANSYS Workbench, where each contact has its own ID, found in Appendix G. The welded connections in the transport frame are defined as the face for each HEM beam and stiffeners, as illustrated in Fig. 8.3.

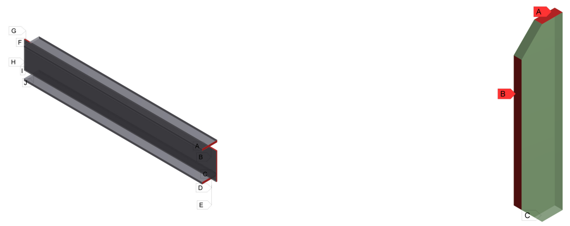

(a) Weld group for HEM beam.

(b) Weld group for stiffeners.

Figure 8.3: Overview over weld group.

The purpose of the stiffeners is to reinforce the locations of force transfer between the barrel and to the transport frame. The stoppers have three different contacts, and the first is bonded to the vessel deck. The contacts to the HEM beam is defined with friction contact, where slide is possible. In particular, non-linear contacts make the model computationally expensive.

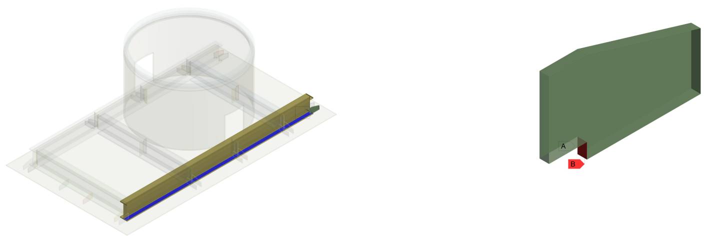

(b) Friction contact - Stiffeners face.

(a) Friction contact - HEM beam face.

Figure 8.4: Friction contacts.

The weld contacts were defined as asymmetric contact to enable the forces and moments extraction used in the weld analysis.

The contacts between parts and their settings are described in Tb. 8.2 for ANSYS model A without weld geometry.

Table 8.2: Contacts - ANSYS model A.

Interface	Contact	Target	Contact type	Formulation
1	Frame	Deck	Frictional	Augmented Lagrange
2	Stoppers	Deck	Bonded	Pure penalty
3	Stoppers	Frame	Frictional	Augmented Lagrange
4	Frame	Frame	Bonded	Pure penalty
5	Frame	Barrel	Bonded	Pure penalty
6	Nacelle dummy	Frame flange	Bonded	Pure penalty
7	Weld	Frame	Bonded	Pure penalty

The weld contacts for the ANSYS model with weld geometry are described in Tb. 8.3.

Table 8.3: Contacts - ANSYS model B.

Interface	Contact	Target	Contact type	Formulation
1	Frame	Deck	Frictional	Augmented Lagrange
2	Stoppers	Deck	Bonded	Pure penalty
3	Stoppers	Frame	Frictional	Augmented Lagrange
4	Frame	Frame	Bonded	Pure penalty
5	Frame	Barrel	Bonded	Pure penalty
6	Nacelle dummy	Frame flange	Bonded	Pure penalty
8	Fillet weld	Frame	Bonded	Pure penalty
8	Weld	Frame	Frictional	Augmented Lagrange

In the ANSYS model B where the weld geometry are included, it also introduced more non-linear contact as illustrated in Fig. 8.5. The contact between the stiffness and HEM beam are defined as friction.

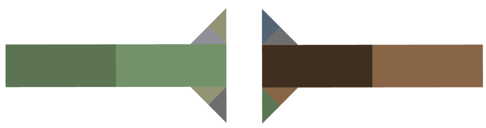

Figure 8.5: ANSYS weld geometry contact.

The friction coefficient is set to 0.05. This is to ensure that the model is converging and also to ensure that the forces and moments are not lowed by the friction between the different parts.

8.4 Boundary conditions

The applied boundary conditions are presented in Fig. 8.6, where the bottom of the vessel deck is constrained against any movement or rotation in the x-direction, y-direction and z-direction. The ship deck is simulated as a rigid deck, where it has been assessed to have sufficient strength to support the loads. The contact between the deck and transport frame is defined as a frictional contact. For supporting the structure against sea motions, stoppers are used as sea-fasting equipment.

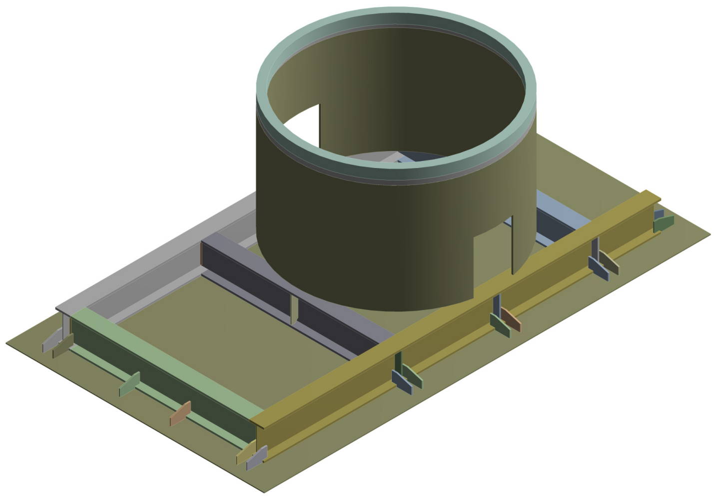

Figure 8.6: Boundary conditions - ANSYS.

8.5 Loads

The forces due to sea transport of the nacelle, where a remote force placed in the CoG represents the nacelle. The loads are applied in two load steps. The first load step is a gravity acceleration in order to get a valid contact between stoppers and transport frame. The second load step is the actual load from inertia and environmental loads. All loads for sea transport are calculated in (Appendix A A.2 - Load-Tool-ANSYS) and copied from Excel to ANSYS Workbench.

8.6 Results

The result presented in the following section includes a presentation of the deformations and the equivalent stresses. Finally, the fatigue damage is calculated in Chapter 9. The deformation of the LC-SEA-FLS-005 is presented in Fig. 8.7.

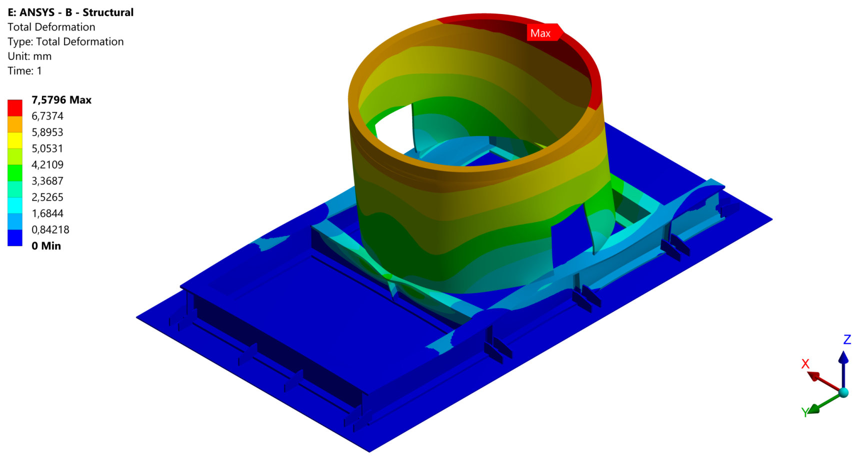

Figure 8.7: ANSYS model B total deformation (Scale 50) - LC-SEA-FLS-005.

The deformation shown in the figure is as predicted that forces from the nacelle weight are moving forward due to the accelerations from rolling. It can also be noted that the deformations are less than the global model. The reason is that main frame is supported in the z-direction by the vessel deck. The total deformation for LC-SEA-FLS-007 is presented in Fig. 8.8.

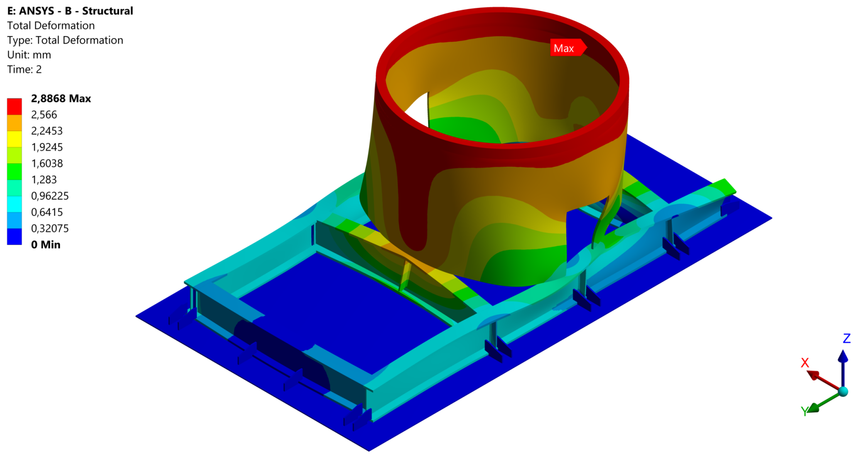

Figure 8.8: ANSYS model B total deformation (Scale 50) - LC-SEA-FLS-007.

Overall the deformations and, thereby, the behaviour of the transport frame act as expected based on rolling accelerations in the y-axis. It can be seen that the forces are pressing the front of the barrel down in z-direction. Where it generated tension at front and opposite is compression, this will shift depending on if it is positive rolling or negative rolling. The maximum equivalent stress for LC-SEA-FLS-005 is presented in Fig. 8.9.

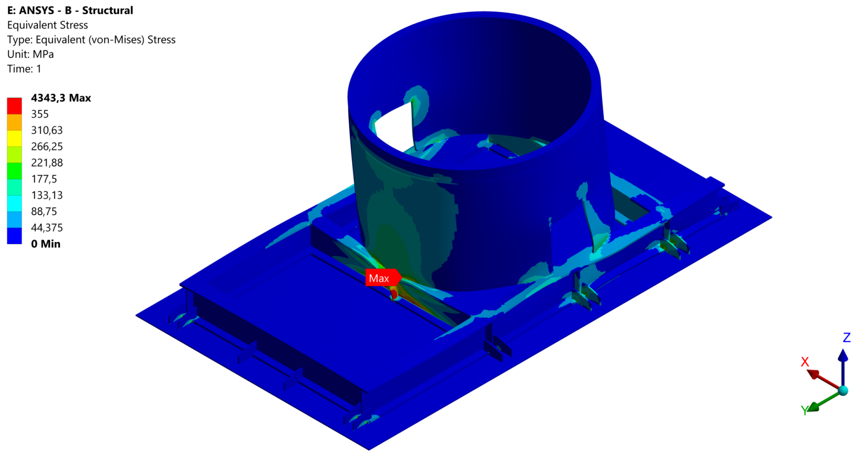

Figure 8.9: ANSYS model A equivalent stress - (Scale 50) - LC-SEA-FLS-005.

In the figure, it can be seen that the peak stress is at the middle of the HEM beam, this is due to the placement of CoG, and the vertical load with positive have. The maximum equivalent stress for LC-SEA-FLS-007 is presented in Fig. 8.10.

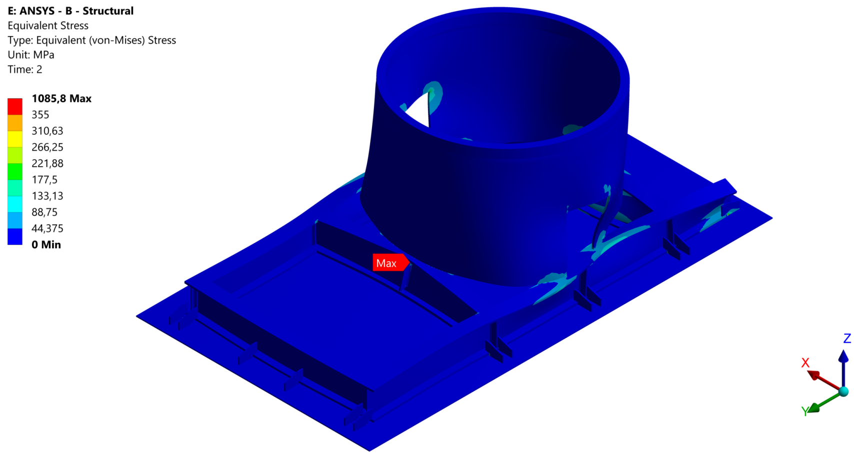

Figure 8.10: ANSYS model A equivalent stress - (Scale 50) - LC-SEA-FLS-007.

The peak stress in the lower load cases is at the same place as the upper load case 8.9, in this case, the rolling accelerations are negative.

Chapter 9

Fatigue verification of weld connection

This chapter gathers all information from the previous chapters and performs the fatigue analysis by Weibull distribution with two parameters. The governing load case defined in Chapter 7. The first parameters is the weld detail, that defined the strength of the weld connection afterwards the different stress approached is used to determine the weld connection with the highest equivalent stress.

9.1 Introduction to fatigue analysis

The results in ANSYS Workbench from the governing load case is used to determine the stress range for fatigue calculations based on the simplified fatigue assessment method.

The ANSYS model A without weld and B with weld geometry has been solved, and the two models are used to analyse the process for fatigue analysis and compare the results. The two different solutions are created where (Solution A) is based on two times the stress to determine the stress range. The second (Solution B) is where the stress range is determined based on the upper and lower load cases.

The first solution A, where the stress range is determined as:

$$\Delta\sigma_w = 2 \cdot \sigma_w \tag{9.1}$$

The second solution B, is to determine the stress range based on upper and lower load case. The resulting forces and moments in x-direction, y-direction and z-direction is determine as:

$$\Delta F_x = |F_{x1} - F_{x2}| \tag{9.2}$$

The different stress approached is explained in Chapter 6 is used on both ANSYS model, thus making it easier to compare and see the advantage of each stress approached.

The first step in the fatigue calculations is to define the properties of each weld based on weld type, size and length, found in Appendix G. There are three welds groups, and the first weld group is the weld connection between the main frame (HEM beam to HEM beam). The second weld group is the connection between the stiffness and HEM beam, and the last weld group is only for ANSYS model B, where the weld geometry is modelled in 3D.

The transport frame has been screening for the weld group with the highest stresses, and this is done by using an Excel sheet, seen in (Appendix A A.3 - ANSYS A - Weld Verification - Without weld) and (Appendix A A.4 - ANSYS B - Weld Verification - With weld). The weld connection selected for fatigue analysis is in ANSYS model A weld group 2 and weld number 4.2. For ANSYS, model B is weld group 3 and weld number 1.7 and 1.8. The weld connection is presented in Fig. 9.1, which is used in the rest of this master thesis to determine the stress range based on a different approach.

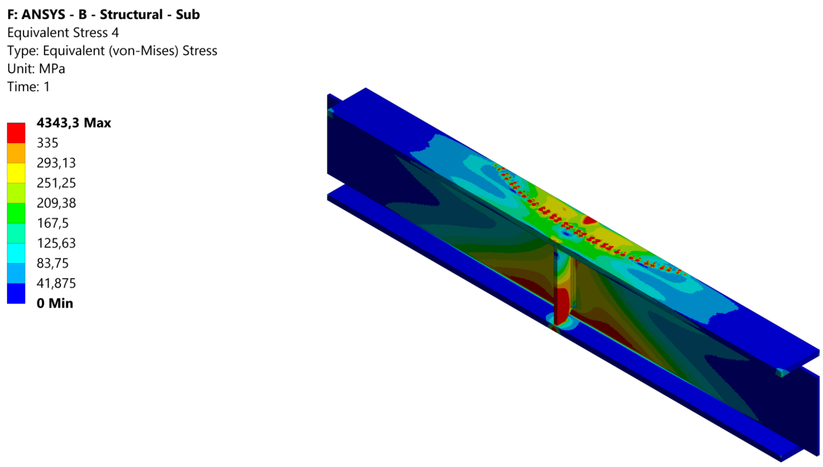

Figure 9.1: HEM beam - Highest equivalent stresses.

9.2 Fatigue equivalent weld stresses

The equivalent weld stresses are often used for fatigue analysis, where the stresses are extracted from the weld contact, presented in Section 9.2. Hence, for the sake of transparency, the weld with the highest equivalent weld stresses is furthermore calculated in Mathcad. This can be found in (Appendix A A.5 - ANSYS A - Equivalent Weld Stress - Without weld) and (Appendix A A.6 - ANSYS B - Equivalent Weld Stress - With weld).

The equivalent weld stresses based on the analytical method is used to determine the stress range for ANSYS model A with solution A. The results are listed in Tb. 9.1 for weld group 2 and weld number 4.2.

Table 9.1: Results for equivalent weld stresses - Solution A - Weld 4.2.

Name	Stress [MPa]
Normal stress	15
Shear stress perpendicular to weld	15
Shear stress along weld	117
Equivalent combined stress	56
Stress range	113

In solution B, where the stress range is based on the upper and lower load case, and the stresses are listed in Tb. 9.2 for weld group 2 and weld number 4.2.

Table 9.2: Results for equivalent weld stresses - Solution B - Weld 4.2.

Name	Stress [MPa]
Normal stress	14
Shear stress perpendicular to weld	14
Shear stress along weld	120
Equivalent combined stress	57
Stress range	57

Based on the stress at the weld throat, it can be seen that the shear stress along the weld is the governing factor in the analytical solution. It can also be noted that the stress range in solution B is lowed by double with determining the stress range based on upper and lower load cases.

For the ANSYS model B, where the weld geometry is included, the forces and moments are extracted from the weld throat plane, illustrated in Fig. 9.2.

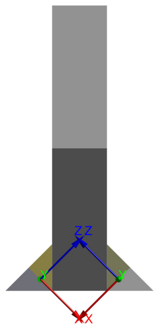

Figure 9.2: Weld geometry - throat plane - ANSYS model B.

The equivalent weld stress with solution A is listed in Tb. 9.3 for weld group 3 and weld number 1.7.

Table 9.3: Results for equivalent weld stresses - Solution A - Weld 1.7.

Name	Stress [MPa]
Normal stress	56
Shear stress perpendicular to weld	56
Shear stress along weld	107
Equivalent combined stress	93
Stress range	186

The stress range is listed in Tb. 9.4 is based on solution B, for weld group 3 and weld number 1.7.

Table 9.4: Results for equivalent weld stresses - Solution B - Weld 1.7.

Name	Stress [MPa]
Normal stress	79
Shear stress perpendicular to weld	79
Shear stress along weld	111
Equivalent combined stress	122
Stress range	122

The same process has been done for weld group 3 and weld number 1.8, in ANSYS model B based on solution A, listed in Tb. 9.5.

Table 9.5: Results for equivalent weld stresses - Solution A - Weld 1.8.

Name	Value [MPa]
Normal stress	51
Shear stress perpendicular to weld	51
Shear stress along weld	107
Equivalent combined stress	86
Stress range	186

The stress range is listed in Tb. 9.6 is based on solution B, for weld group 3 and weld number 1.8.

Table 9.6: Results for weld equivalent stresses - Solution B - Weld 1.8.

Name	Stress [MPa]
Normal stress	73
Shear stress perpendicular to weld	73
Shear stress along weld	111
Equivalent combined stress	115
Stress range	115

Based on the results, it can be seen when including the weld geometry in the ANSYS model, where the forces and moments are exacted at the weld throat in 45 deg plane that the stresses are higher than when not include the weld geometry and project the stress at the weld throat plane. The remarkable is in ANSYS model A with solution A is that stress range is 113 MPa, and for solution B stress range is only 57 MPa. In the ANSYS model A, when the gravity is included and multiplying the upper load case with two, this also means that the gravity is double. The point is to remove the gravity for the load case if the designer wants to multiply the stress by two for the stress range. This has been tested based on ANSYS model A, where the gravity is equal to one. The results are listed in Tb. 9.7. The solution can be found (Appendix A A.5 - ANSYS A - Equivalent

Table 9.7: Results for weld equivalent stresses - Solution A - Weld 4.2 - no gravity.

Name	Stress [MPa]
Normal stress	13
Shear stress perpendicular to weld	13
Shear stress along weld	117
Equivalent combined stress	43
Stress range	86

It can be noted that the stress range is 86 MPa if the gravity is equal to one and compared with the stress range in ANSYS model A based on solution B, where the stress range was 53 MPa.

9.3 Fatigue hot spot stresses

The hot spot method is used to determine the stress at the weld toe on both the left and right side of the stiffness. The parameters used in hot spot methods is listed in Tb. 9.8. The hot spot calculations can be found in (Appendix A A.7 - Hot spot method).

Table 9.8: Hot spot parameters HEM profile.

Name	Symbol	Distance [mm]
Plate thickness	t	21
Read-out 1	$L_{0.5t}$	10.5
Read-out 2	$L_{1.5t}$	31.5

The stress is extracted at read-out one and read-out two with the linearized equivalent stress in ANSYS Workbench on both sides of the weld geometry. The first hot spot stress is based on ANSYS model A is without the weld geometry, results are listed in Tb. 9.9.

Table 9.9: Results for hot spot - Solution A.

ANSYS model	Side	Stress [MPa]
ANSYS model A	Right	415
ANSYS model A	Left	409

In the ANSYS model B with the weld geometry, the results from Solution B is based on the stress range is listed in Tb. 9.10.

Table 9.10: Results for hot spot - Solution B.

ANSYS model	Side	Stress [MPa]
ANSYS model B	Right	353
ANSYS model B	Left	358

The hot spot methods are recommended for calculating the structural stress at the weld toe. It can note that the hot spot stress at the weld toe is almost three times higher than in the analytical solution. The reason is that the linearised equivalent stress values from ANSYS is positive, and it does not account if the structure is in tension or compression.

9.4 Fatigue effective hot spot stresses

The effective hot spot stress is determined based on the principal stress, where two different alternative methods. The first methods are named Method ALT-A where the stress at the weld toe is taken as 0.5t and 1.5t. The second method ALT-B, where the stress is only read out at 0.5t. The effective hot spot stresses are combined with the principal stresses presented in Section 9.4. The parameters used in both methods are listed in Tb. 9.11. The effective hot spot calculations can be found in (Appendix A A.8 - Effective hot spot method).

Table 9.11: Hot spot parameters - Method ALT-A.

Name	Symbol	Distance [mm]
Plate thickness	t	21
Distance 1	$L_{0.5t}$	10.5
Distance 2	$L_{1.5t}$	31.5

The results from the effective hot spot stress ALT-A for ANSYS model A without weld is listed in Tb. 9.12.

Table 9.12: Results for effective hot spot stresses - ANSYS model A - Method ALT-A.

Name	Side	Stress [MPa]
1. Principal stress	Right	278
2. Principal stress	Right	-3
Effective stress	Right	278
1. Principal stress	Left	287
2. Principal stress	Left	-10
Effective stress	Left	287

The results from the effective hot spot stresses ALT-A for ANSYS model B with weld is listed in Tb. 9.13,

Table 9.13: Results for effective hot spot - ANSYS model B - Method ALT-A.

Name	Side	Stress [MPa]
1. Principal stress	Right	317
2. Principal stress	Right	28
Effective stress	Right	317
1. Principal stress	Left	387
2. Principal stress	Left	0
Effective stress	Left	378

The results from the effective hot spot stresses ALT-B for ANSYS model A with weld is listed in Tb. 9.14,

Table 9.14: Results for principal stresses - ANSYS model A - Method ALT-B.

Name	Side	Stress [MPa]
1. Principal stress	Right	180
2. Principal stress	Right	-3
Effective stress	Right	180
Effective stress with 1.12	Right	202
Effective stress without 1.12	Right	180
1. Principal stress	Left	186
2. Principal stress	Left	-9
Effective stress	left	186
Effective stress with 1.12	Left	208
Effective stress without 1.12	Left	186

The results from the effective hot spot stress ALT-B for ANSYS model B with the weld geometry is listed in Tb. 9.14.

Table 9.15: Results for principal stresses - ANSYS model B - Method ALT-B.

Name	Side	Stress [MPa]
1. Principal stress	Right	196
2. Principal stress	Right	17
Effective stress	Right	193
Effective stress with 1.12	Right	217
Effective stress without 1.12	Right	193
1. Principal stress	Left	235
2. Principal stress	Left	-1
Effective stress	left	235
Effective stress with 1.12	Left	263
Effective stress without 1.12	Left	235

The largest stress is used to determine the principal stress, which is then used to determine the effective stress. It can be seen that the stress used in the effective hot stress method used the normal stress and shear stress to determine the principal. In this case, it can either be positive values for tension and negative values for compression. This method is recommended compared to using the hot spot method with linearized equivalent stress.

9.5 Damage analysis

The damage is based on the simplified fatigue assessment, presented in Section 5.5. It should be noted that the parameters used in the fatigue calculations are comparison reasons only. The Weibull parameter that has been considering is listed in Tb. 9.16. The fatigue can be found in (Appendix A A.9 - Fatigue damage) and (Appendix A A.10 - Fatigue DNV Simplified).

Table 9.16: Design parameters for Weibull distribution.

Name	Symbol	Value	Unit
Weibull shape parameter	h	1.10	-
Roll period	T_R	6	Sec
Exposure for each heading direction	E_{xp}	10	%
Load cycles in Weibull distribution	n_0	10^4	-
Number of cycles per head direction	N_{ch}	6.10^3	-
Frequency, Roll	V_0	0.16	Hz

The S-N curve used in fatigue damage calculation is based on W3 letter used in equivalent stress approached and for the hot spot approached, the D letter is used. The parameters are listed in Tb. 9.17.

Table 9.17: Design parameters for S-N curve.

S-N curve letter	Symbol	Value
W3	m_1	3
W3	$\log(\bar{a}_1)$	10.97
D	m_1	3
D	$\log(\bar{a}_1)$	12.16

The purpose of his study is to mainly compare the stress approach. The calculated fatigue damage for ANSYS model A is listed in Tb. 9.18.

Table 9.18: Calculated damage - ANSYS model A.

Stress approach	S-N	Stress	Weibull stress	Fatigue damage
Equivalent weld stress (2x)	W3	113.20	15.84	0.00
Equivalent weld stress (Gravity = 1) (2x)	W3	87.00	12.10	0.00
Equivalent weld stress (Range)	W3	57.4	8.03	0.00
Hot Spot left 0.5t - 1.5t (Range)	D	415	58.01	0.09
Hot Spot right 0.5t - 1.5t (Range)	D	409	57.19	0.09
Hot Spot left 0.5t (Range)	D	415	52.55	0.07
Hot Spot right 0.5t (Range)	D	409	51.85	0.06
Effective method A Right	D	278	38.94	0.03
Effective method A left	D	287	40.09	0.03
Effective method B with 1.12	D	202	28.21	0.01
Effective method B without 1.12	D	180	25.19	0.01

The calculated fatigue damage for ANSYS model B is listed in Tb. 9.19.

Table 9.19: Calculated damage - ANSYS model B.

Stress approach	S-N	Stress	Weibull stress	Fatigue damage
Equivalent weld stress left (2x)	W3	185.9	26.01	0.01
Equivalent weld stress left (Range)	W3	122.4	17.13	0.00
Equivalent weld stress right (2x)	W3	185.9	26.01	0.01
Equivalent weld stress right (Range)	W3	114.9	16.08	0.00
Hot Spot left 0.5t - 1.5t (Range)	D	353	49.36	0.00
Hot Spot right 0.5t - 1.5t (Range)	D	358	50.08	0.00
Hot Spot left 0.5t (Range)	D	415	46.20	0.00
Hot Spot right 0.5t (Range)	D	409	46.72	0.00
Effective method A Right	D	317	44.37	0.00
Effective method A left	D	378	52.93	0.00
Effective method B right with 1.12	D	217	30.32	0.00
Effective method B right without 1.12	D	193	27.07	0.00
Effective method B left with 1.12	D	263	36.76	0.00
Effective method B left without 1.12	D	235	32.83	0.00

Throughout the fatigue calculations, different theories were applied, and results were obtained in Tb. 9.18 for ANSYS model A and TB. 9.19 ANSYS model B. The table shows the damage contribution for each of the stress approached. By looking at the results, it can be mentioned that the approach used for determining the stress influence the Weibull stress. The reason for this is to see whether or not there are any consistencies between the methods applied. Secondly, the fatigue damage in the weld toe and at the weld throat are compared and discussed. It can be seen that the stresses at the weld throat calculated based on the analytical method in equivalent weld stress are below the yield and where the stresses at the weld toe are above the yield point. The method used to determine the stress range has a significant impact on the fatigue damage.

Chapter 10

Discussion

The main scope of the present report was to study different fatigue assessments approach based on the simplified fatigue damage by a two parameters Weibull distribution.

It must be noted that the analyses were performed on an example of a transport frame in the beam software Autodesk ROBOT and ANSYS Workbench. Furthermore, the model showed to be very promising compared to the traditional transport frames.

By implementing the global analysis in beam software, where several simulations were run and results in terms of reactions, deformations, forces, moments and code check of the defined members cross-sections was analysed. A global beam model is an essential tool that can be used to identify which load cases are necessary to validate the details in the transport equipment. When modelling complex transport equipment and conditions, it is time-consuming to achieve a model that represents reality exactly. During the simplified global model, various decisions were made based on assumptions on how the structure would behave. Some of the choices made during the modelling are discussed in this Section 7.

The governing load case was identified based on the global beam model in ROBOT. The criteria for selecting the load case was based on the highest utilisation cross-section and the reactions forces in the supports and can be found in Section 7.6.

The advantage of using the global model is that it is very fast to get an overview of beams ratio based on buckling according to Eurocode. It must be noted that buckling analysis depends on the length of the members. If the members are defined as two sections, it affects the buckling capacity. Suppose if all load cases as ULS-A, ULS-B for sea and road was included in the global model. The designer could easily change the selected cross-section until acceptable results are reached. The disadvantage is that if the designer is not used to model equipment in global model with beam elements. It requires that the designer makes an assumption that allowed the forces to transmit through the structure.

The methods used for calculation the stress range was based on the equivalent weld stresses, hot spot stresses and effective hot spot stresses. The modelling techniques used do also vary based on the approach. The stress range calculations are done by use of finite element model without or with the weld geometry. The application of the investigated fatigue damage showed that the application of local approaches for determining the stress range was time-consuming and complex to update. If the modelled weld fails under fatigue, the designer must update the geometry and rerun the model until an approved designer is obtained, as illustrated in Appendix B.

Before the equipment could be solved in ANSYS, it is necessary to set up the model as described in Chapter 8. The designer must define all contacts as bonded or friction, where model mistake and convergence problems can occur due to non-linear contact. The primary non-linear contact in transport equipment is the bolted interface between the wind turbine components and transport equipment, and this will increase the solving time drastically.

In the ANSYS model A without the weld geometry, the solving time was 22 min with only non-linear contact between the vessel deck and main frame and between the stoppers and transport frame.

The ANSYS model B with the weld geometry, for each weld geometry implementing in the ANSYS model, intruded one additional non-linear contact. The solving time for ANSYS model B was 4 hours.

The determining of the stress range two approached was analysed, where (Solution A) is based on two times the stress. For (Solution B), the stress range is determined based on both the upper and lower load cases.

Equivalent weld stress is an analytical method, where the designer used the nodal stress in the defined weld contact in ANSYS. Before the designer can get the forces and moments, each weld contact is defined manually with a local coordinate system. It is a time-consuming process, and a model mistake can occur during this process. These methods allow the designer to verifies all weld connection in the structure. When this process is finished, the designer can copies the forces and moments from ANSYS and past in Excel, where it automatically determines the equivalent weld stress. When the 3D model from Inventor is linked to ANSYS Workbench, it makes the update smooth regarding change of the plate thickness, rerun the ANSYS model, and copies the new results in Excel.

The hot spot stress is a simple task to perform in ANSYS, where two-path is made parallel with the weld based on the two read-out points. The membrane and bending stress are linearised based on equivalent stress. The hot spot method determined the stresses at the weld toe, where the main challenge is the mesh settings. It is hard to mesh alignment with the weld geometry. It must be noted that the mesh size in the finite element model may influence the hot spot stresses when the mesh becomes finer As the stress goes higher. It is difficult to determine if the stress is tension or compression in ANSYS Workbench. This has a significant consequence of the stress range determined based on the hot spot method.

The effective hot spot stress is combined with principal stress, where the stress is taken either at 0.5t or combined of 0.5t and 1.5t away from the weld toe. This method gives a more precise solution than the hot spot stress based on linearised equivalent stress. The reason is that the effective hot spot stress used the normal stresses and shear stress, and in this case, it can either be positive or negative values. The designer does not need to take into account if the detail is in tension or compression. The effective hot spot stress is recommended if the designer do not have defined all weld contact as described in Section 8.3. This method can be used in the areas where the stresses are above the yield point.

The nominal stress method could have been used based on the stress in the global model, this would have allowed the designer to lower the nominal stresses by changing the cross-section in the model before it is imported to ANSYS Workbench. It is challenging to update the ANSYS model if the designer wants to minimise the nominal stress.

The methodology used today based on solution A, where the equivalent weld stress is multiplied by two, is a conservative approach. If the designer wants to use this approved, it is recommended to set the gravity equal to one in the FLS load case. Based on the results, it may first be mentioned that the analytical method generally predicted lower damage when the stress range is based on the upper and lower load case.

Chapter 11

Conclusion

The objective of this master thesis was to investigate the methods used for calculating the stress range used in fatigue analysing. This has been done with the evaluating of the differences stresses range methods recommended by DNVGL. The fatigue damage is then calculated by the simplified fatigue assessment based on two parameters Weibull distribution.

It can be concluded that the global beam model was used in the analysing of the process of transport equipment, presented in Chapter 7. This ensures that the selected cross-section of the members is verified based on the Eurocode check. This can be found in Section 7.6. The benefit of the global beam model was that it reduces the time spent solving complex ANSYS models because only the governing load case was analysed in ANSYS. This has inspired to utilise of the global model in the features projects, and it is recommended that more structure designer are learning and understanding the concept of using beam software.

It has been discovered that the driven factor in fatigue assessment is the flowing parameters weld properties, wave parameters, vessel dimensions and methods used to determine the stress range.

It can be concluded from the results obtained that the methodology used today based on solution A is a conservative approach to determine the fatigue damage, where the equivalent weld stress is multiplied by two based on the upper load case.

Based on the results in Chapter 9, it can be noted that if equivalent weld stress is used for fatigue calculations, it is recommended to set the gravity equal to one. This will allow the designer only to solve one load case for determining the stress range. It is recommended to use solution B, where the upper and lower load cases are used to determine the stress range. Solution B gives a more realistic picture of the stress range, and it will lower the overall weld size and optimise the weight of the transport frame.

The tool developed under this master thesis, listed in Appendix A, had a great impact on the flow with defined the load combinations and made it a better experience to use ROBOT and ANSYS Workbench. It also made the analysis process for fatigue calculations more smooth.

It is noticed that the study could be more accurate if the shape parameters in the Weibull distribution were taken into account, shown in Section 5.5. Suppose a more detailed analysis of the wave could have a significant impact on the fatigue damage. This could, for example, be metocean analysis, which would give a more precise picture of the wave parameters and wind parameters.

This will set the basis for future work, which should lead to creating an accurate fatigue damage of transport equipment or make the design process a better experience. Presenting a selection of topics of which future research is suggested in order to improve the knowledge:

- Hydrodynamic analysis
- Sea sate analysis
- Weibull parameters (Shape)
- Examine whether it is tension or compression stress in ANSYS
- Use of shell element in ANSYS Workbench model

Bibliography

[1] Siemens Gamesa. *SG 14-222 DD*. URL: https://www.siemensgamesa.com/products-and-services/offshore/wind-turbine-sg-14-222-dd (visited on 05/09/2020).

[2] Siemens Gamesa. *Siemens wind power in CuxHaven*. URL: https://www.siemensgamesa.com/explore/journal/offshore-wind-power-in-cuxhaven (visited on 08/09/2020).

[3] windpowerengineering. *Siemens Gamesa fully implements its "roll-on, roll-off" offshore logistics concept*. URL: https://www.windpowerengineering.com/siemens-gamesa-fully-implements-its-roll-on-roll-off-offshore-logistics-concept.

[4] bigliftshipping. *BigNews*. URL: https://www.bigliftshipping.com/assets/data/bignews/BigNews_31.pdf.

[5] Fred. Olsen Windcarrier. *Jack-ups, Windcarrier fleet*. URL: https://windcarrier.com/fleet.

[6] K.J. Rawson and E.C. Tupper. *Basic Ship Theory*. 5. ed. ISBN 0-7506-5396-5. Longman group limited, 2001.

[7] Siemens Gamesa. *Taiwanese 376 MW Formosa 2 offshore wind project set for launch*. URL: https://www.siemensgamesa.com/newsroom/2019/10/191028-siemens-gemesa-of-tw-formosa-2 (visited on 01/10/2020).

[8] Thomas Lykke Andersen. *Coastal, Offshore and Port Engineering*. 2020.

[9] Edward R. Bohnart. *Welding Principles and Practices*. 5. ed. ISBN 978-0-07-337386-7. McGraw-Hill Eduaction, 2018.

[10] John Hicks. *Welded design theory and practice*. 1. ed. ISBN 1-85573-537-7. Abington Publishing, 2000.

Appendix A

Virtual files

The virtual files such as the ANSYS, ROBOT, AutoCAD and Excel for loads calculations and Mathcad for fatigue calculations. All files can be accessed on the following onedrive link. Please note, that in order to access the files, it is necessary to have a Aalborg University email login.

Appendix A

A elaborate description of the content is:

- Appendix A.1 - Load-Tool-ROBOT
- Appendix A.2 - Load-Tool-ANSYS
- Appendix A.3 - ANSYS A - Weld Verification - Without weld
- Appendix A.4 - ANSYS B - Weld Verification - With weld
- Appendix A.5 - ANSYS A - Equivalent Weld Stress - Without weld
- Appendix A.6 - ANSYS B - Equivalent Weld Stress - With weld
- Appendix A.7 - Hot spot method
- Appendix A.8 - Effective hot spot method
- Appendix A.9 - Fatigue damage
- Appendix A.10 - Fatigue DNV Simplified
- Appendix A.11 - Autodesk Inventor - Inventor Transport frame
- Appendix A.12 - Autodesk AutoCAD - AutoCAD global model
- Appendix A.13 - Autodesk ROBOT - ROBOT Global v10
- Appendix A.14 - ANSYS Workbench - ANSYS Model V5

Appendix B

Flowchart

The process used for design of steel structure is presented in Fig. B.1.

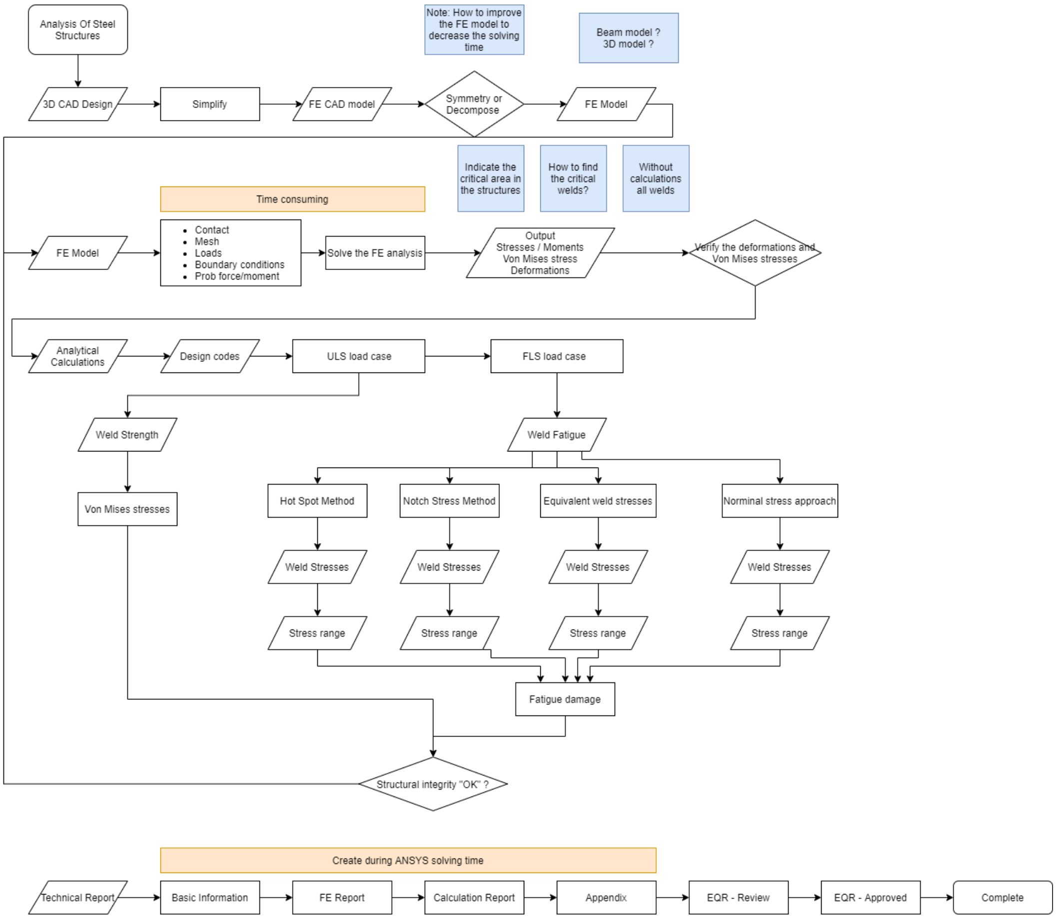

Figure B.1: Flowchart.

Appendix C

Rolling loads

The input for the motions is the time period for rolling and pitching and the angle and then convert it into angular accelerations. The rolling accelerations are given in Eq. C.1 by using the equation for rolling accelerations:

$$Roll_{acc} = Roll_{angle} \cdot \left(\frac{2\pi}{T_{Roll}} \right)^2 \tag{C.1}$$

The accelerations are defined based on the fixed global vessel coordinate system, presented in Section 2.1. To calculate the accelerations in the combined CoG of transport frame and nacelle, when the accelerations in CoG of the vessel are available, theory of motion analysis for vessel motion is applied.

Based on ship motion theory, the effective accelerations at each point consist of the linear rigid-body motions of the vessel, component accelerations due to the rotational accelerations, and effective accelerations due to gravity in combination with the maximum roll angle and pitch angle. When using the default motion criteria, the following simplified approach can be used to determine the forces for rolling, illustrated in Fig. C.1 a simple presentation for determining the transverse and vertical forces. The same approach can be used for the pitching of the vessel.

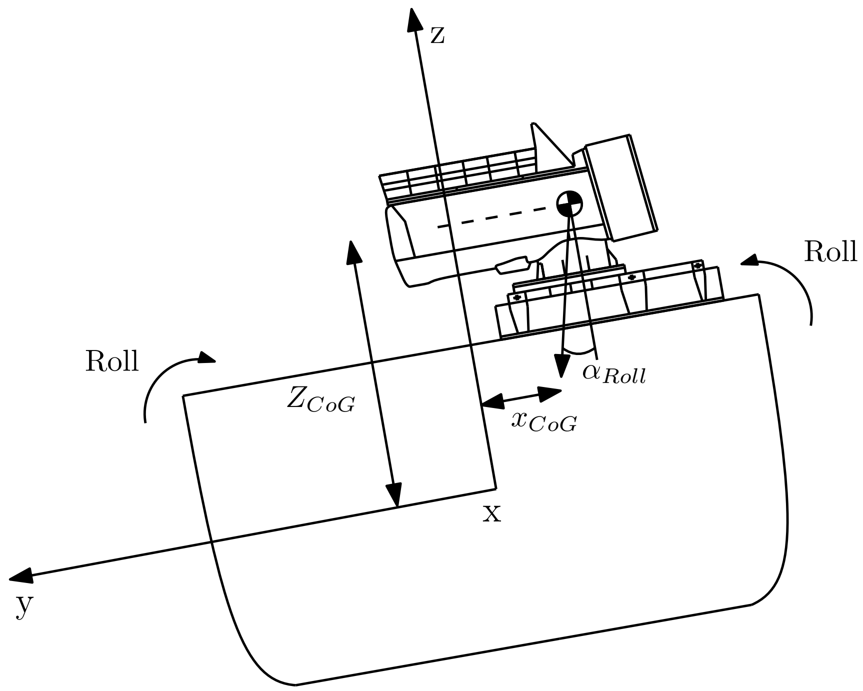

Figure C.1: Forces action on Centre of gravity.

The static force for the self-weight in transverse direction is given as:

$$Static_x = Self_{weight} \cdot \sin(\alpha_{roll}) \tag{C.2}$$

Where the $Self_{weight}$ is the weight of transport frame and nacelle. The rolling angle is defined as α_{roll}

The static force for the self-weight in vertical direction is given as:

$$Static_z = Self_{weight} \cdot \cos(\alpha_{roll}) \tag{C.3}$$

The dynamic force in transverse direction due to angular acceleration is given as:

$$Dynamic_x = Self_{weight} \cdot \left(\frac{2 \cdot \pi}{T_{Roll}}^2\right) \cdot Z_{CoG} \cdot \alpha_{roll} \tag{C.4}$$

Where T_{roll} is the rolling period and Z_{CoG} is the distance from x-axis to CoG.

The dynamic force in vertical direction due to angular acceleration is given as:

$$Dynamic_z = Self_{weight} \cdot \left(\frac{2 \cdot \pi}{T_{Roll}}^2\right) \cdot X_{CoG} \cdot \alpha_{roll} \tag{C.5}$$

The distance in x direction is defined as X_{CoG}

The combined heave and roll forces in transverse direction is given as:

$$Combined_x = Self_{weight} \cdot a_{heave} \cdot \sin\alpha(_{roll}) \tag{C.6}$$

The combined heave and roll forces in vertical direction is given as:

$$Combined_z = Self_{weight} \cdot a_{heave} \cdot \cos(\alpha roll) \tag{C.7}$$

Where the heave accelerations is defined as a_{heave}.

The total forces in the transverse direction are the static combined with the dynamic force given as:

$$Total_z = Static_x + Dynamic_x + Combined_x \tag{C.8}$$

The total forces in vertical direction are the static combined with the dynamic force given as:

$$Total_z = Static_z + Dynamic_z + Combined_z \tag{C.9}$$

Appendix D

Wind load

The first parameter that is requite for calculated the wind forces action during offshore transport is the wind speed profile. The wind speed are determine based on the height of the structure z and the wind profile, is given as [DNV-RP-C205, Sec. 2.3.2.11]:

$$U_{T,z} = U_{10} \cdot \left(1 + 0.137 \cdot \ln\left(\frac{z}{H}\right) - 0.047 \ln\left(\frac{T}{T_{10}}\right)\right) \tag{D.1}$$

Where U_{10} is the 10 minute mean wind speed at height H, T_{10} is 10 minutes and z is the height of the objected. T is the averaging time and defined in DNVGL-ST-N001, sec. 3.6.4.2, the averaging times depends on the length or the calculations.

According to [DNV-RP-C205, Sec. 5.2.1], the basic wind pressure q is given in Eq. D.2:

$$q = \frac{1}{2} \cdot \rho_a \cdot U_{T,z}^2 \tag{D.2}$$

Where ρ_a is the mass density of air at 15C and $U_{T,z}$ is the wind velocity at a height defined as z above the mean water level.

The wind force action on a objected is given in Eq. D.3 [DNV-RP-C205, Sec. 5.3.1]:

$$F_W = C_e \cdot q \cdot A \cdot \sin\alpha \tag{D.3}$$

Where C_e is the effective shape coefficient, A is the projected area of the wind turbine components and transport frame and α is the angle between the wind direction and the axis of the exposed surface. The shape parameter are defined in [DNV-RP-C205, Table 5-3]

Appendix E

Guide - Global model work in ROBOT

This appendix is a guild, that shows how to create a global model in Autodesk AutoCAD and how to import the global model in ROBOT. The 3D model is based on solid model in Autodesk Inventor. This method also work with Siemens NX or SolidWorks. The first step is to create a 3D model in Autodesk Inventor, presented in Fig. E.1.

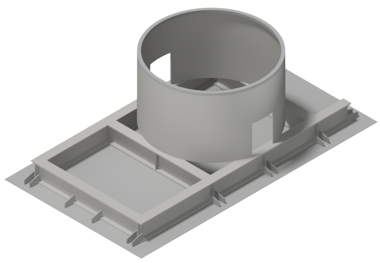

Figure E.1: Autodesk Inventor - 3D model transport frame.

When the model is ready for FE, the 3D model must be exported as igs format. The igs format, create each part as a body, this will make it easier to model the beam element for centre-line of each beams. The user need to export the CAD file, as illustrated in Fig. E.2.

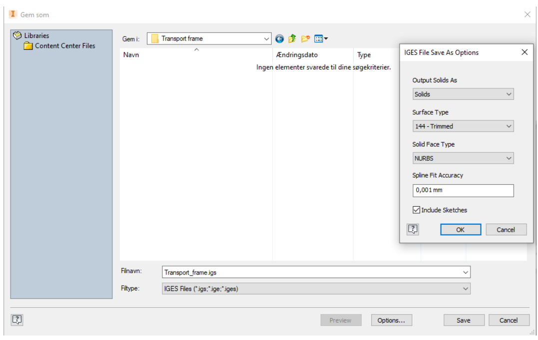

Figure E.2: Autodesk Inventor - Export igs format.

When Inventor has created the igs file, it can now be imported in Autodesk AutoCAD, as illustrated in Fig. E.6.

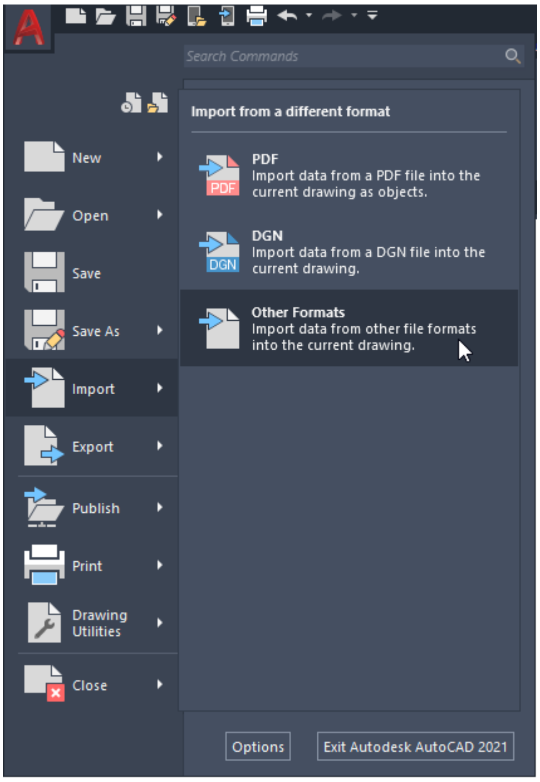

Figure E.3: Autodesk AutoCAD - Import igs format.

The global model is created based on the 3D CAD model from Inventor, depicted in Fig. E.7.

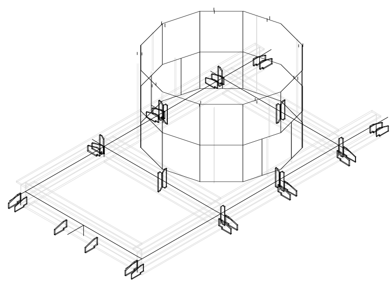

Figure E.4: Autodesk AutoCAD global model with Inventor model.

The next step is to deleted the bodys, so only the global model with beam elements is imported in ROBOT, depicted in Fig. E.5.

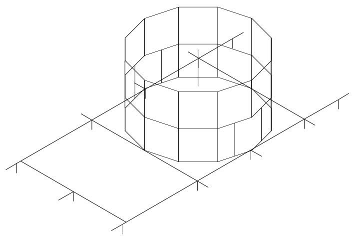

Figure E.5: Global model in Autodesk AutoCAD.

When opening the software Autodesk ROBOT, the user must select project type. In the guide, Frame 3D design is used to the global model.

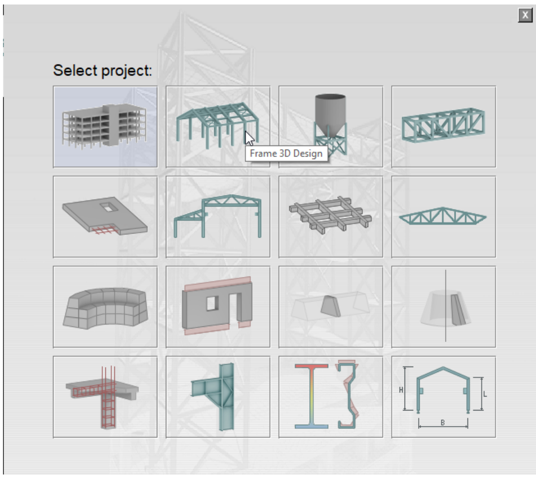

Figure E.6: Autodesk ROBOT - Project settings.

Before the beam element model from AutoCAD can be open in ROBOT, the user must change the dimension settings from meter to millimeter. The settings is found under Job Preferences, shown in Fig. E.7.

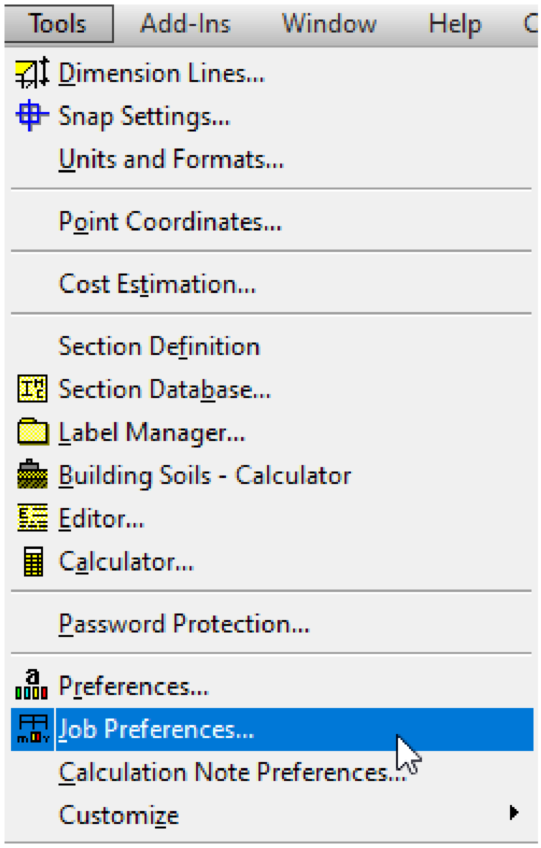

Figure E.7: Autodesk - Job Preferences.

The settings is shown in Fig. E.8.

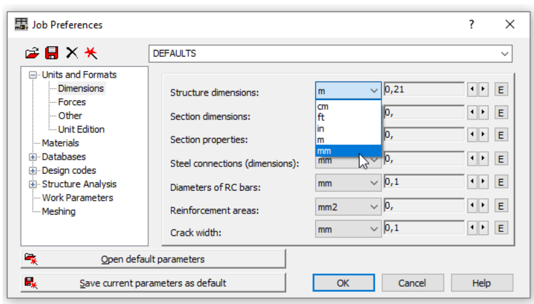

Figure E.8: Autodesk - Job Preferences settings.

The AutoCAD file is now open in ROBOT, shown in Fig. E.9

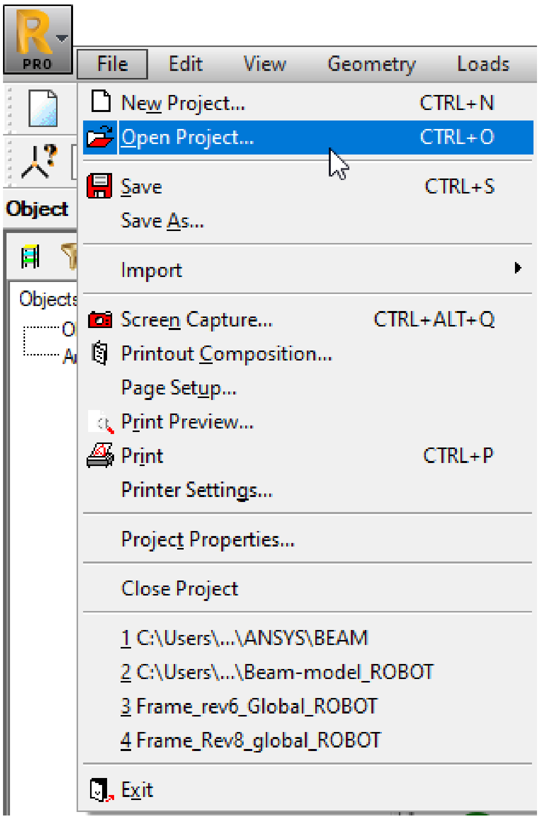

Figure E.9: Autodesk ROBOT - Open AutoCAD file in ROBOT.

The user need to browse, shown in Fig. E.8

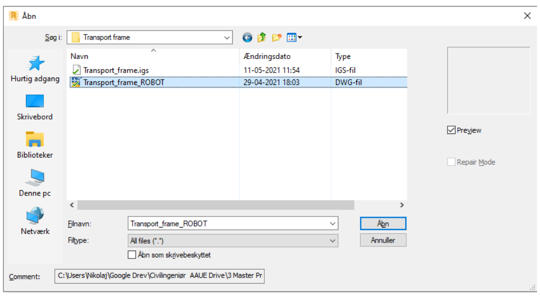

Figure E.10: Autodesk ROBOT - Open AutoCAD file in ROBOT.

The discretiztion parameters are shown in Fig. shown in Fig. E.11

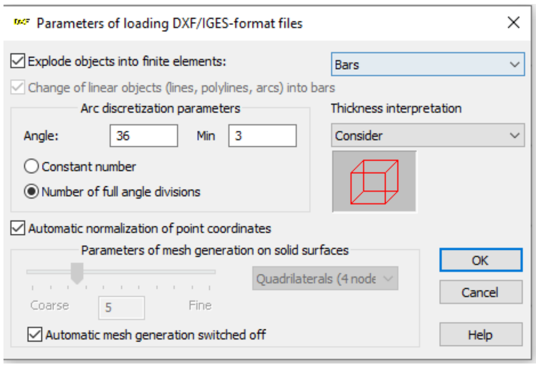

Figure E.11: Autodesk ROBOT - Default Discretiztion.

The global model in Autodesk ROBOT, shown in Fig. E.12, is now ready for defined cross-section for each beam, supports and load types.

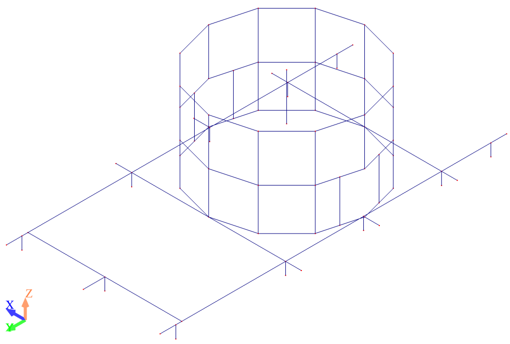

Figure E.12: Global model in ROBOT.

Appendix F

Material

The material used for the transport is steel, and the behaviour is isotropic. The stress-strain diagram for steel is illustrated in Fig. F.1. The elastic is where the material returns to its original shape after the acting load. In this zone, stress and deformation have a linear proportional relationship. The stress at this point is defined as the yield stress σ_y. The value of the stress where the material start to fracture is referred to as the ultimate stress σ_u

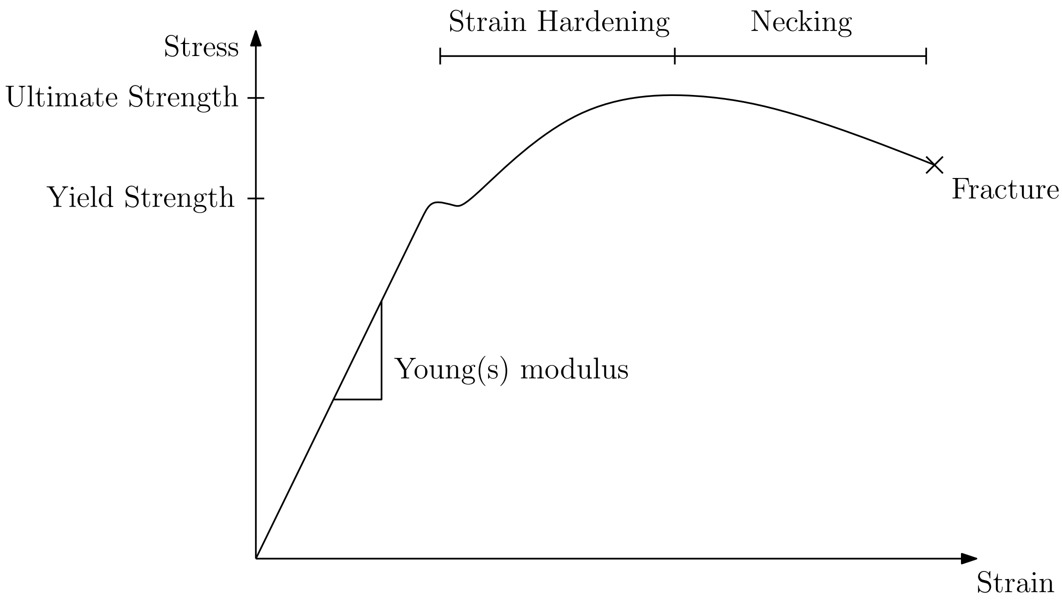

Figure F.1: Stress-strain curve for isotropic material.

When designing transport frame or machine it is important consideration if the it is allowed to behave in plastic manner. When designing a machine it is not allowed to behave in a plastic zone. The reasons is the tolerances between the machine parts. In this project only elasticity is allowed.

Poisson(s) ratio is a measure of the lateral contraction of a material when under tensile stress in the longitudinal direction. Poisson(s) ratio varies from 0.2 for some grades of cast iron to 0.45 for some grades of polythene.

Appendix G

Weld category

There are three welds groups, the first weld group is the weld connection between the main frame (HEM beam to HEM beam). The second weld group is the connection between the stiffness and HEM beam and the last weld group is only for ANSYS model B, where the weld geometry is modeled in 3D.

Table G.1: Weld GP 1 - HEM beam - Model A - [mm].

Weld group	Weld No.	Weld type	Weld size	Weld length	Plate Thickness
1	1.1	Partial penetration	15	305	40
1	1.2	Fillet weld	15	114	21
1	1.3	Fillet weld	15	540	21
1	1.4	Fillet weld	15	114	21
1	1.5	Partial penetration	15	305	40

For model B, where the fillet weld geometry is included the weld for main frame is listed Tb. G.2.

Table G.2: Weld GP 1 - HEM beam - Model B - [mm].

Weld group	Weld No.	Weld type	Weld size	Weld length	Plate Thickness
1	1.1	Partial penetration	15	305	40
1	1.2	Fillet weld	15	114	21
1	1.3	Fillet weld	15	540	21
1	1.4	Fillet	15	114	21
1	1.5	Partial penetration		305	40

The second groups of weld is the stiffness for model A is listed in Tb. G.3.

Table G.3: Weld GP 2 - Stiffness - Model A - [mm].

Weld group	Weld No.	Weld type	Weld size	Weld length	Plate Thickness
2	1.1	Fillet weld	15	65	40
2	1.2	Fillet weld	15	400	21
2	1.3	Fillet weld	15	65	40

The second groups of weld is the stiffness for model B is listed in Tb. G.4.

Table G.4: Weld GP 2 - Stiffness - Model B - [mm].

Weld group	Weld No.	Weld type	Weld size	Weld length	Plate Thickness
2	1.1	Fillet weld	15	65	40
2	1.2	Fillet weld	15	400	21
2	1.3	Fillet weld	15	65	40

The last weld group three is only for model B, where the the fillet weld geometry is include in the ANSYS model, listed in Tb. G.5.

Table G.5: Weld GP 3 - Fillet geometry - Model B - [mm].

Weld group	Weld No.	Weld type	Weld size	Weld length	Plate Thickness
2	1.1	Fillet weld	15	65	40
2	1.2	Fillet weld	15	400	21
2	1.3	Fillet weld	15	65	40

When all weld details is defined, the weld stress can be estimating based on the different fatigue assessment for stress range.